Inorganic Chemistry

Article

pubs.acs.org/IC

Unprecedented Tris-Phosphido-Bridged Triangular Clusters with 42 Valence Electrons. Chemical, Electrochemical and Computational Studies of their Formation and Stability

Tiziana Funaioli,[†] Piero Leoni,*[,†] Lorella Marchetti,[†] Alberto Albinati,[‡] Silvia Rizzato,[‡] Fabrizia Fabrizi de Biani,[§] Andrea Ienco,[∥] Gabriele Manca,[∥] and Carlo Mealli*[,∥]

[†]Dipartimento di Chimica e Chimica Industriale dell'Università di Pisa, Via Risorgimento 35, I-56126 Pisa, Italy

[‡]Dipartimento di Chimica dell'Università di Milano, Via C. Golgi 19, I-20133 Milano, Italy

[§]Dipartimento di Chimica dell'Università di Siena, Via A. Moro, I-53100 Siena, Italy

[∥]Istituto di Chimica dei Composti OrganoMetallici, Via Madonna del Piano 10, I-50019 Sesto Fiorentino (Firenze), Italy

Supporting Information

ABSTRACT: This paper presents the synthesis and structural characterization of the unprecedented tris-phosphido-bridged compounds $Pt_3(\mu\text{-}PBu^t_2)_3X_3$ (X = Cl, Br, I), having only 42 valence electrons, while up to now analogous clusters typically have 44e$^-$. The new species were obtained by an apparent bielectronic oxidation of the 44e$^-$ monohalides $Pt_3(\mu\text{-}PBu^t_2)_3(CO)_2X$ with the corresponding dihalogen X_2. Their X-ray structures are close to the D_{3h} symmetry, similarly to the 44e$^-$ analogues with three terminal carbonyl ligands. The products were also obtained by electrochemical oxidation of the same monohalides in the presence of the corresponding halide. In a detailed study on the formation of $Pt_3(\mu\text{-}PBu^t_2)_3I_3$, the redox potentials indicated that I_2 can only perform the first monoelectronic oxidation but is unsuited for the second one. Accordingly, the 43e$^-$ intermediate $[Pt_3(\mu\text{-}PBu^t_2)_3(CO)_2I]^+$ was ascertained to play a key role. Another piece of information is that, together with the fully oxidized product $Pt_3(\mu\text{-}PBu^t_2)_3I_3$, the transient 44e$^-$ species $[Pt_3(\mu\text{-}PBu^t_2)_3(CO)_3]^+$ is formed in the early steps of the reaction. In order to extract detailed information on the formation pathway, involving both terminal ligand substitutions and electron transfer processes, a DFT investigation has been performed and all the possible intermediates have been defined together with their associated energy costs. The profile highlights many important aspects, such as the formation of an appropriate couple of 43e$^-$ intermediates having different sets of terminal coligands, and suitable redox potentials for the transfer of one electron. Optimizations of 45e$^-$ associative intermediates in the ligand substitution reactions indicate their possible involvement in the redox process with reduction of the overall energy cost. Finally, according to MO arguments, the unique stability of the 42e$^-$ phosphido-bridged Pt_3 clusters can be attributed to the simultaneous presence of three terminal halides.

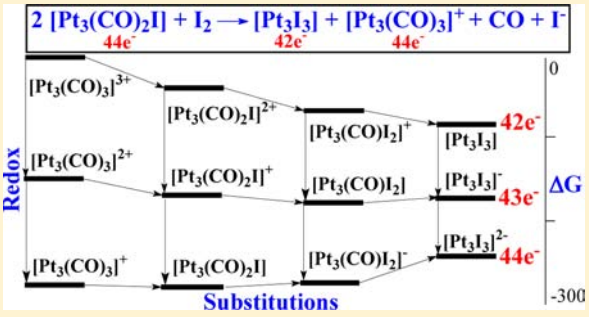

1. INTRODUCTION

The seminal papers published 40 years ago by J. Chatt and P. Chini reported the synthesis of new derivatives of general formula $Pt_3(\mu\text{-}CO)_3(PR_3)_n$ (n = 3−4).[1] Since then, many other triangular platinum clusters (TPCs) with different bridging and terminal ligands have been prepared and characterized. Today more than 100 X-ray structures with a Pt_3 triangular core have been deposited in the CCDC archives,[2] often with non-equivalent Pt−Pt distances. Depending on the valence electron count (VEC), the bond orders may vary between one and zero, and also for the same VEC. In fact, the strengths of the Pt−Pt linkages may be influenced by factors such as the nature of the bridging and terminal ligands. The great interest in TPCs was initially stimulated by studies on the relations between structure and VEC in late transition metal clusters[3] and by the search of analogies with metal surfaces.[4] Interestingly, these derivatives are also building blocks for clusters with a higher nuclearity, which can be achieved through the addition of other mononuclear fragments, to give tetrahedra,[5] butterflies,[6] or trigonal bipyramids.[7] A single metal atom can link together two TPCs to give a Pt_3MPt_3 sandwich,[8] with eclipsed or staggered orientation of the triangles.[9,10] Moreover, it is well-known that the stepwise oxidation of the $[Pt_{3n}(CO)_{6n}]^{2-}$ Chini clusters results in the progressive stacking of $Pt_3(CO)_3(\mu\text{-}CO)_3$ units giving rise to infinite chains, which can be discontinuous, semicontinuous or continuous, depending on the size of the cluster anion and on the organic or inorganic countercation.[9d,e] This is not the case of TPCs with bulky phosphido bridges, although we have shown that removal of one bridge from the

Received: January 31, 2013
Published: March 28, 2013

   dx.doi.org/10.1021/ic400251y | Inorg. Chem. 2013, 52, 4635−4647

$Pt_3(\mu\text{-}PR_2)_3$ core allows perpendicular bonding between the naked Pt−Pt linkage to form hexanuclear species with a dibridged tetrahedral core and an interesting redox behavior.[11] More recently, we and others have used the TPCs as the precursors of bi- or polycluster molecular assemblies, in which two or more cluster units are interconnected not through new metal−metal bonds but by organic, inorganic or organometallic spacers.[11a−c,12]

The VEC of TPCs varies between 42 and 48 and depends on the set of ligands and on the oxidation states of the metals. The $42e^-$ species of general formula $Pt_3(\mu\text{-}L)_3L'_3$ contain terminal L′ ligands such as CO, RNC, PR_3 and three neutral π-acceptor bridges (L = CO, RNC, SO_2, R_2E, with E = C, Si, Sn). The formal $Pt^0{}_3$ skeleton is normally equilateral with three short Pt−Pt linkages (2.61−2.82 Å).[1,3−10,13] Other $42e^-$ species instead involve three Pt(II) ions which, given their preference for the local 16 electron configuration, allow single Pt−Pt bonds consistently with an adjusted EAN rule.[2] A matchless type of $42e^-$ TPC is $[Pt_3(\mu\text{-dppm})_3(\mu_3\text{-CO})]^{2+}$ (dppm = bis-diphenylphosphinomethane),[14] which is the precursor of many tris-dppm bridged derivatives with a higher electron count. Clusters with VEC = 44 are numerous, and some of them are derived from the mentioned $42e^-$ precursors $Pt_3(\mu\text{-}L)_3L'_3$[15] or $[Pt_3(\mu\text{-dppm})_3(CO)]^{2+}$,[7d,16] upon addition of a further two electron donor. The most common $44e^-$ TPCs are however the tris-phosphido-bridged ones of general formula $[Pt_3(\mu\text{-}PR_2)_3(L)_3]^{+}$[11g,17,18] or $Pt_3(\mu\text{-}PR_2)_3(L)_2X$.[12a,c,17−20] In general, the Pt−Pt separations are longer than single bonds, with distances around 3 Å. Also, depending on the nature of the terminal ligands, the triangle can be equilateral or isosceles. In particular, a single terminal anion may force the elongation of the opposite Pt−Pt linkage even up to a breaking point (3.61 Å in the case of H^-),[19b] while the other two approach single bond orders. Remarkable cases of cluster core isomerism have been also reported for different crystallizations of clusters with formula $Pt_3(\mu\text{-}PR_2)_3(L)_2X$ (X = aryl anion) with either an "open" or a "closed" triangular shape.[11a,20c] TPCs with VEC = 46[18,21] or 48[22,23] are often based on the $Pt_3(\mu\text{-dppm})_3$ core with some ligands perpendicular to the Pt_3 plane. Some $48e^-$ species can be described as formed by three L_4Pt^{II}-d^8 fragments, whose out-of-plane *trans*-ligands are the oxygen atoms of bridging carboxylates.[23] In these cases, the application of the EAN rule based on the $18e^-$ metal configuration predicts three single Pt−Pt bonds, which indeed are among the shortest found (2.51−2.61 Å).

In this paper we describe the synthesis and spectroscopic, crystallographic, electrochemical and computational characterization of the new derivatives $Pt_3(\mu\text{-}PBu^t_2)_3X_3$ (X = Cl, Br, I)], the first tris-phosphido bridged species with VEC = 42 and a Pt_3^{6+} triangular core. Since the stability of $42e^-$ TPCs with three phosphido bridges is unprecedented, the role of the three terminal halide ligands in favoring depopulation of a key frontier MO has to be clarified. From the mechanistic viewpoint, it is important to evaluate the TPC stabilization upon oxidation and the energies associated with different possible steps. To this aim, a detailed DFT investigation has been carried out to monitor the electronic evolution of the system and determine a realistic profile for the overall reaction.

2. RESULTS AND DISCUSSION

2.1. Syntheses. We have recently shown that the reaction of the tricarbonyl cation $[Pt_3(\mu\text{-}PBu^t_2)_3(CO)_3]^+$, $[\mathbf{Pt_3(CO)_3}]^+$ {$\mathbf{Pt_3}$ = $Pt_3(\mu\text{-}PBu^t_2)_3$}, with an excess of halides affords the $44e^-$ substitution derivatives $Pt_3(\mu\text{-}PBu^t_2)_3(CO)_2X$ ($\mathbf{Pt_3(CO)_2Cl}$, X = Cl; $\mathbf{Pt_3(CO)_2Br}$, X = Br; $\mathbf{Pt_3(CO)_2I}$, X = I).[19a] In CH_2Cl_2 solution, these clusters undergo two sequential monoelectronic oxidations at potentials close to +0.3 and +0.9 V (vs SCE) (Table 1). The first step has the features of chemical reversibility on the time scale of cyclic voltammetry, while the second oxidation is coupled to chemical complications.[19a] The data suggested that suitable terminal ligands may stabilize tris-phosphido bridged Pt_3 derivatives with VEC < $44e^-$, previously unknown. Indeed, the chemical oxidation of $\mathbf{Pt_3(CO)_2I}$ with 1 equiv of I_2, carried out at room temperature in dichloromethane solution, affords the triangular $42e^-$ cluster $Pt_3(\mu\text{-}PBu^t_2)_3I_3$, $\mathbf{Pt_3I_3}$ (Scheme 1), in a high yield (77%). The analogous derivative $Pt_3(\mu\text{-}PBu^t_2)_3Br_3$, $\mathbf{Pt_3Br_3}$, was also prepared by chemical oxidation of $\mathbf{Pt_3(CO)_2Br}$ with Br_2 in 74% yield, although the reaction had to be performed at low temperature (−20 °C) and required a more careful control of the stoichiometry. In fact, less controlled conditions gave mixtures of various derivatives, among which only a very low amount of the desired product was identified. The attempted synthesis of the trichloro derivative $Pt_3(\mu\text{-}PBu^t_2)_3Cl_3$, $\mathbf{Pt_3Cl_3}$, by chemical oxidation of $\mathbf{Pt_3(CO)_2Cl}$ with Cl_2 was unsuccessful.

Table 1. Formal Electrode Potentials (V, vs SCE) and Peak-to-Peak Separations (mV) in 0.2 M $[Bu^n_4N][PF_6]/CH_2Cl_2$ Solution

	$E^{\circ\prime}$ (ΔE_p)[a]	
cluster	$44e^-/43e^-$	$43e^-/42e^-$
	2−/−	−/0
$\mathbf{Pt_3Cl_3}$	−1.32 *(75)*	−0.74 *(65)*
$\mathbf{Pt_3Br_3}$	−1.29 *(65)*	−0.74 *(60)*
$\mathbf{Pt_3I_3}$	−1.24 *(75)*	−0.72 *(70)*
	−/0	0/+
$\mathbf{Pt_3(CO)I_2}$	−0.47[b]	+0.06[b]
	0/+	+/2+
$\mathbf{Pt_3(CO)_2Cl}$	+0.31 *(60)*	+0.91[c] *(70)*
$\mathbf{Pt_3(CO)_2Br}$	+0.29 *(60)*	+0.88[c] *(70)*
$\mathbf{Pt_3(CO)_2I}$	+0.28 *(70)*	+0.86[c] *(70)*
	+/2+	2+/3+
$[\mathbf{Pt_3(CO)_3}]^+$	+1.13 *(90)*	+1.56[d]

[a]Measured at 0.1 V s^{-1}. [b]Extrapolated from the correlation of Figure 2 (see below). [c]Partially chemically reversible process. [d]Coupled to fast chemical reactions.

Scheme 1. Possible Pathways in the Transformation from $\mathbf{Pt_3(CO)_2I}$ and to $\mathbf{Pt_3I_3}$

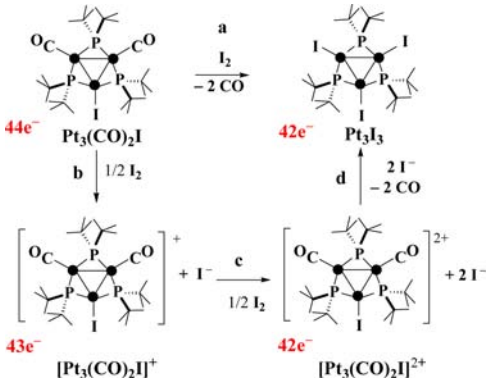

dx.doi.org/10.1021/ic400251y | *Inorg. Chem.* 2013, 52, 4635−4647

However, Pt_3Cl_3 could be obtained, analytically pure although in very small yields (11%), by reacting $Pt_3(CO)_2Cl$ with an equimolar amount of PCl_5. The latter reactant more efficiently delivers Cl_2 upon the equilibrium $PCl_5 \leftrightarrows PCl_3 + Cl_2$. In this way, large local concentrations of Cl_2, which otherwise induce massive decomposition, are avoided.

Also, Pt_3I_3 and Pt_3Br_3 could be obtained, respectively, by $Pt_3(CO)_2I$ and $Pt_3(CO)_2Br$ solutions, upon exhaustive electrolysis at their first oxidation potential in the presence of an excess of the corresponding halide anion (see Experimental Section). Under similar conditions, the monochloro species $Pt_3(CO)_2Cl$ did not transform into Pt_3Cl_3. In view of these results, the order $Pt_3I_3 > Pt_3Br_3 > Pt_3Cl_3$ was assumed for the thermal stability of these species. Pt_3I_3 (violet), Pt_3Br_3 (pink) and Pt_3Cl_3 (yellow) were isolated as air-stable solids and were shown by X-ray diffraction to have crystallographic 3-fold symmetry. The latter is maintained in solution as shown by multinuclear (^1H, $^{13}C\{^1H\}$, $^{31}P\{^1H\}$ and $^{195}Pt\{^1H\}$) NMR spectroscopy. The interpretation of the NMR spectra is straightforward (see Experimental Section) and will not be further discussed here. A thermally stable salt of the $43e^-$ cation $[Pt_3(CO)_2I]^+$, later shown to be a key intermediate in the formation of Pt_3I_3, was obtained by treating a CH_2Cl_2 solution of $Pt_3(CO)_2I$ with 1 equiv of $[Cp_2Fe]PF_6$. $[Pt_3(CO)_2I]PF_6$ was isolated as a brown-greenish solid, which analyzes correctly and exhibits a ν_{CO} absorption at 2062 or 2072 cm^{-1} in the solid state or in acetone solution, respectively, shifted at higher wavenumbers in comparison to $Pt_3(CO)_2I$ (2024 cm^{-1} in CH_2Cl_2). Due to the paramagnetic nature of this $43e^-$ species, we observed only a very broad signal at δ = 12 ppm in the ^1H NMR spectrum, and even broader, scarcely informative, resonances in the ^{31}P and ^{195}Pt NMR spectra. The species converts back cleanly to $Pt_3(CO)_2I$ when reacted with 1 equiv of Cp_2Co in CH_2Cl_2 solution.

2.2. Electrochemistry. The $42e^-$ clusters Pt_3X_3 undergo two separate one-electron reductions in CH_2Cl_2 solution, both possessing features of reversibility in the cyclic voltammetric time scale (Figure 1a). The two waves are fully reversible [$(i_p)_{red}/(i_p)_{ox}$ = 1.0 for scan rates, ν, between 50 and 500 mV s^{-1}] and diffusion controlled [$(i_p)_{red}/\nu^{1/2}$ = constant], and the peak-to-peak separations, ΔE_p, are not far from the theoretical value of 59 mV. In the cyclic voltammetry of Pt_3I_3 also a single monoelectronic, partially chemically reversible, oxidation process was observed at +1.43 V, indicating the attainment of a $41e^-$ species. The formal electrode potentials for the redox changes exhibited by the Pt_3X_3 species, and the related $Pt_3(CO)_2X$[19a] and $[Pt_3(CO)_3]CF_3SO_3$,[11g] are compiled in Table 1. Upon bulk electrolysis at the first reduction process (E_w = −1.0 V) the purple solution of Pt_3I_3 turns green and the cyclic voltammetric tests, performed on the resulting monoanion $[Pt_3I_3]^-$, confirm the profile already observed for Pt_3I_3. This definitely validates the stability of the $43e^-$ species $[Pt_3I_3]^-$ (Figure 1b). Conversely, the bulk electrolysis at the second electron addition (E_w = −1.3 V) induces decomposition of the cluster, as confirmed by an intense peak at E = +0.43 V, which can be ascribed to the oxidation of the I^- anion released in solution.[24]

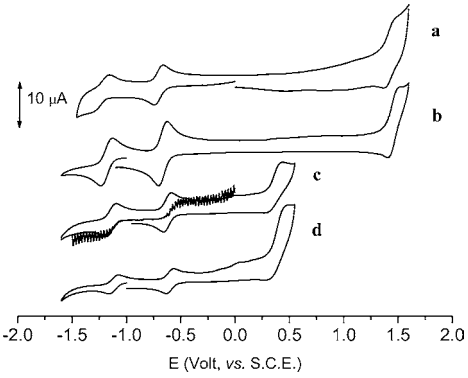

Figure 1. Cyclic voltammogram recorded at a platinum electrode in CH_2Cl_2 solution of (a) Pt_3I_3 (1.1×10^{-4} M), (b) $[Pt_3I_3]^-$ generated by bulk electrolysis, (c–d) after bulk electrolysis of Pt_3I_3 at the second reduction process: (c) one electron addition, (d) exhaustive electrolysis. $[Bu^n_4N][PF_6]$ (0.2 mol dm^{-3}) supporting electrolyte. Scan rate 0.2 V s^{-1}.

The current remains high also after the formal addition of one electron to the $43e^-$ TPC, while hydrodynamic voltammetry with periodical renewal of the diffusion layer indicates that the most reduced species $[Pt_3I_3]^{2-}$ is unattainable. As a general trend in Table 1, the separations between the monoelectronic redox peaks for each given species are in the range 430–580 mV. Conversely, any CO/I^- replacement shifts each redox peak of 700–850 mV toward the cathodic region. For instance, the $44/43e^-$ process involving the different couples $[Pt_3(CO)_3]^{+/2+}$, $[Pt_3(CO)_2I]^{0/+}$ and $[Pt_3I_3]^{2-/-}$ occurs at +1.13, +0.28 and −1.24 V, respectively. The difference between the last two potentials is nearly doubled with respect to the first couple of values, consistently with the potential existence of the unobserved intermediates $[Pt_3(\mu\text{-}PBu^t_2)_3(CO)I_2]^{-/0}$, $[Pt_3(CO)I_2]^{-/0}$. Eventually, consumption of Pt_3I_3 from the solution was observed (Figure 1d). Comparable trends are detected for the $43/42e^-$ process.

Indeed, as shown by the plot in Figure 2, there is a linear correlation [$E^\circ_1 = 1.104 - 0.786n$ and $E^\circ_2 = 1.586 - 0.764n$ for

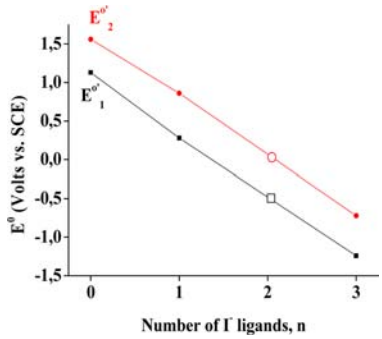

Figure 2. Linear correlation between redox potentials and number of terminal iodide ligands in the species $[Pt_3(\mu\text{-}PBu^t_2)_3(CO)_{3-n}I_n]^{x-n}$ (n = 0–3, x = 1–3). $E^{\circ\prime}_1$ (■) and $E^{\circ\prime}_2$ (●) refer to $44/43e^-$ and $43/42e^-$ redox couples, respectively. Unfilled symbols correspond to the extrapolated positions of the experimentally undetected redox couples $[Pt_3(CO)I_2]^{x-2}$ with x = 1/2 and 2/3, respectively.

E°_1 (R = −0.99962 and $P = 3.753 \times 10^{-4}$) and for E°_2 (R = −0.9996 and $P = 3.9723 \times 10^{-4}$)][25] between the experimental redox potentials and the n number of iodide ligands in the clusters $[Pt_3(CO)_{3-n}I_n]^{x-n}$ (n = 0–3, x = 1–3). In this manner, also the redox potentials for the unobserved species $Pt_3(CO)I_2$ can be estimated as −0.47 and +0.06 V for the $44/43e^-$ ($[Pt_3(CO)I_2]^{-/0}$) and the $43/42e^-$ ($[Pt_3(CO)I_2]^{0/+}$) transformations, respectively.

dx.doi.org/10.1021/ic400251y | Inorg. Chem. 2013, 52, 4635–4647

2.3. Crystal Structures of Pt_3X_3. Single crystal X-ray determinations were carried out for the 42e$^-$ clusters $\mathbf{Pt_3Cl_3}$, $\mathbf{Pt_3Br_3}$ and $\mathbf{Pt_3I_3}$. The compounds are isomorphous (space group $P6_3/m$), hence only the $\mathbf{Pt_3I_3}$ structure is shown in Figure 3. Selected geometrical parameters of the three clusters are reported in Table 2, with those of the known 44e$^-$ cation $[\mathbf{Pt_3(CO)_3}]^+$ for comparative purposes.

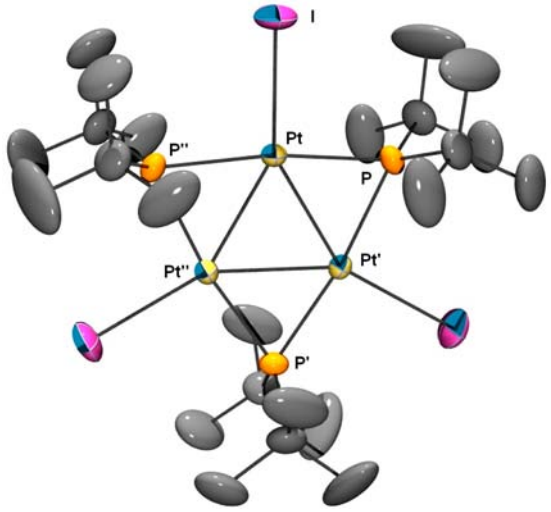

Figure 3. An Ortep view of $\mathbf{Pt_3I_3}$ with thermal ellipsoids drawn at 30% probability. The H atoms are omitted for clarity.

Table 2. Bond Lengths (Å) and Angles (deg) for Pt_3I_3, Pt_3Br_3, Pt_3Cl_3 and $[Pt_3(CO)_3]^+$[a]

	Pt_3X_3			
	X = I	X = Br	X = Cl	$[Pt_3(CO)_3]^+$
Pt–Pt′	2.5893(3)	2.5786(3)	2.5818(3)	2.961(1) 2.982(1)
Pt–P	2.293(1)	2.286(1)	2.287(2)	2.307(4)
Pt–P′	2.299(1)	2.291(1)	2.293(2)	2.314(4)
Pt–X	2.6277(4)	2.4545(6)	2.332(3)	
Pt′– Pt–Pt″	60.0*	60.0*	60.0*	59.76(2) 60.49(3)
X–Pt–P	93.67(3)	93.67(4)	94.4(1)	
X–Pt–P″	94.97(3)	94.91(4)	94.2(1)	
X–Pt–Pt′	149.47(2)	149.48(2)	150.0(1)	
X–Pt–Pt″	150.53(2)	150.52(2)	150.0(1)	
Pt–P–Pt′	68.64(3)	68.58(3)	68.62(7)	79.7(1) 80.5(1)
P–Pt–Pt′	55.79(3)	55.81(3)	55.81(6)	50.0(4) av
P–Pt′–Pt	55.57(3)	55.61(3)	55.57(6)	
P–Pt–P″	171.36(3)	171.42(3)	171.37(7)	160.1(9)

[a]Primed and doubly primed atoms are obtained from those unprimed by the symmetry operations: (i) $1-y, x-y, z$; (ii) $1-x+y, 1-x, z$. *Symmetry imposed value.

The $\mathbf{Pt_3X_3}$ clusters share a 3-fold axis and the perpendicular mirror plane, with only one independent atom of the type Pt, and X plus a "PBu^t" moiety. The resulting molecular symmetry is D_{3h} (see below). The Pt–Pt separations are very similar (in the range 2.589–2.579 Å), only those in $\mathbf{Pt_3I_3}$ being slightly but significantly (>5σ) longer than in the other analogues. Most remarkable is the large ~0.4 Å shortening of the Pt–Pt bond lengths with respect to similar 44e$^-$ species, such as the cation $[\mathbf{Pt_3(CO)_3}]^+$ (av 2.97 Å).[11g] Such a difference is consistent with an increase of the Pt–Pt bond order from 0.66 to 1.0, as it is theoretically predictable on depopulating the higher σ^* Pt_3 level of these frameworks.[26]

The Pt–P distances are similar in all the 42e$^-$ structures, with an average value of 2.289(4) Å, which is shorter than in the 44e$^-$ species $[\mathbf{Pt_3(CO)_3}]^+$ (2.310(4) Å). An explanation for this trend will be offered in the Theoretical Studies. The terminal Pt–X separations at 2.332(3), 2.4545(6) and 2.6277(4) Å in $\mathbf{Pt_3Cl_3}$, $\mathbf{Pt_3Br_3}$ and $\mathbf{Pt_3I_3}$, respectively, follow the expected trends based on the atomic radii and are in the lower range of distances found in the few known Pt clusters with terminal halides.[11d,16f,19a,27] We also note minor asymmetries in the Pt–P separations (at the 3σ level) and small deviations from the ideal D_{3h} values of bond angles (<1.5 deg, see Table 2) that lower the molecular symmetry.

2.4. Experimental Observations and Their Implications for Possible Mechanisms. The simplest conceivable route to $\mathbf{Pt_3I_3}$ is the concerted oxidative addition of I_2 to $\mathbf{Pt_3(CO)_2I}$ accompanied by expulsion of the carbonyl ligands [path a in Scheme 1]. Although this process is evaluated by DFT calculations (vide infra) to be as exoergonic as −50 kcal mol^{-1}, such an interpretation was abandoned because inconsistent with the experimental evidence of 43e$^-$ intermediates, unaccounted for by a concerted mechanism. Another reasonable conjecture is that $\mathbf{Pt_3I_3}$ forms through stepwise oxidations of $\mathbf{Pt_3(CO)_2I}$ by I_2 to give the 42e$^-$ dication $[\mathbf{Pt_3(CO)_2I}]^{2+}$ (steps b and c in Scheme 1). The simultaneously formed iodide anions would eventually substitute the carbonyl ligands to give $\mathbf{Pt_3I_3}$. Such a hypothesis was also discarded, on the basis that the reduction potential of I_2 in organic solvents (+0.43 V),[24] being intermediate between the +0.28 and +0.86 V values of the first and the second oxidation of $\mathbf{Pt_3(CO)_2I}$ (see Table 1), is inadequate for the second oxidation. More detailed information on the mechanism was provided by the electrolysis of a CH_2Cl_2 solution of $\mathbf{Pt_3(CO)_2I}$ also containing 0.2 M $[Bu^n{}_4N]PF_6$. The imposed potential (E_w = +0.4 V) was suited only for the first anodic step.

After the exhaustive one-electron oxidation, cyclic voltammetry (CV) showed only the profile of the monocation $[\mathbf{Pt_3(CO)_2I}]^+$, which is stable throughout the electrolysis time. Importantly, 15 min after the addition of a 3-fold excess of $[Bu^n{}_4N]I$, the CV indicated the presence of equimolar amounts of $\mathbf{Pt_3I_3}$ and $[\mathbf{Pt_3(CO)_3}]^+$ characterized by their well-known profiles (see Table 1).[19a] The formation of the 1:1 mixture was confirmed by the ^{31}P NMR signals of the corresponding species.

These appeared (still in rough 1:1 ratio, and together with those of the reactant $\mathbf{Pt_3(CO)_2I}$ at δ_P = 171.8 and 64.6 ppm) also in the early stages of its chemical oxidation with I_2. In the long run, the ^{31}P NMR signals of $\mathbf{Pt_3(CO)_2I}$ and $[\mathbf{Pt_3(CO)_3}]^+$ (δ_P = 154.6 ppm) vanished, leaving only the resonance of $\mathbf{Pt_3I_3}$ at 405.3 ppm. In fact, while $\mathbf{Pt_3I_3}$ accumulates, $[\mathbf{Pt_3(CO)_3}]^+$ returns in circle in agreement with the right shift of eq 1, which is also the basis for the synthesis of $\mathbf{Pt_3(CO)_2I}$.[19a] The sequence of the possible events is illustrated in Scheme 2.

$$[\mathbf{Pt_3(CO)_3}]^+ + I^- \leftrightarrows \mathbf{Pt_3(CO)_2I} + CO \quad (1)$$

Another informative series of experiments was carried out in an acetone solution of the 43e$^-$ compound $[\mathbf{Pt_3(CO)_2I}]PF_6$, prepared and isolated as described above. The species is stable for several hours at room temperature, as confirmed by the IR spectra (ν_{CO} = 2072 cm^{-1}), whereas an added equimolar

dx.doi.org/10.1021/ic400251y | Inorg. Chem. 2013, 52, 4635–4647

Scheme 2. Evolution of the Redox/Substitution Processes

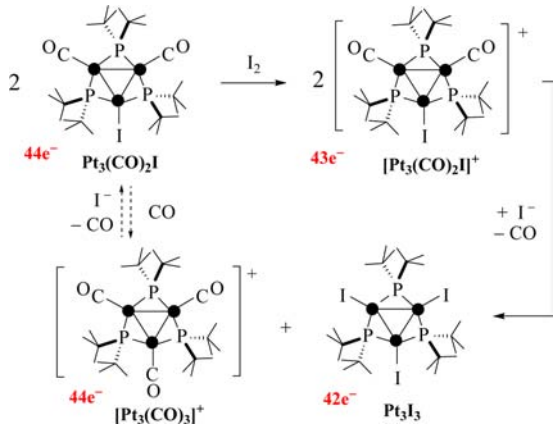

amount of $[Bu^n_4N]I$ rapidly generates the known 1:1 mixture of $[Pt_3(CO)_3]^+$ and Pt_3I_3.

An excess of $[Bu^n_4N]I$ quantitatively converts $[Pt_3(CO)_3]^+$ into $Pt_3(CO)_2I$ within a few minutes, while, after the addition of $[Bu^n_4N]I$ and I_2, only Pt_3I_3 was observed in solution. The above experimental data support the key role of the 43e$^-$ intermediate $[Pt_3(CO)_2I]^+$ in generating both $[Pt_3(CO)_3]^+$ and Pt_3I_3 (see eq 2), but do not provide any clear indication on the nature of the redox reactants, nor on the chronological order of the substitutions/redox steps. A significant answer in this respect is provided by the computational approach (*vide infra*).

$$2[Pt_3(CO)_2I]^+ + I^- \leftrightarrows [Pt_3(CO)_3]^+ + Pt_3I_3 + CO \quad (2)$$

By assuming that electron transfer occurs before CO/I$^-$ scrambling, two identical 43e$^-$ $[Pt_3(CO)_2I]^+$ cations would participate in a disproportion-like process leading to the 42e$^-$ and 44e$^-$ species, $[Pt_3(CO)_2I]^{2+}$ and $Pt_3(CO)_2I$ (eq 3a), followed by the CO/I$^-$ substitutions shown in eqs 3b and 3c.

$$\begin{array}{ll} \text{a)} & 2\,[Pt_3(CO)_2I]^+ \leftrightarrows Pt_3(CO)_2I + [Pt_3(CO)_2I]^{2+} \\ \text{b)} & [Pt_3(CO)_2I]^{2+} + 2\,I^- \leftrightarrows Pt_3I_3 + 2\,CO \\ \text{c)} & Pt_3(CO)_2I + CO \leftrightarrows [Pt_3(CO)_3]^+ + I^- \end{array} \quad (3)$$

$$2\,[Pt_3(CO)_2I]^+ + I^- \leftrightarrows [Pt_3(CO)_3]^+ + Pt_3I_3 + CO$$

While eqs 3 would have the advantage of excluding the unrealistic 43/42e$^-$ oxidation of $[Pt_3(CO)_2I]^+$ by I_2, the process is unlikely. For instance, the formation of the equimolar mixture of Pt_3I_3 and $[Pt_3(CO)_3]^+$ in the early steps of the reaction is in contrast with their formation in the two independent equilibria 3b and 3c. In particular, the latter equilibrium must be shifted toward $Pt_3(CO)_2I$ in the presence of an excess of I$^-$, also consistent also with the +3.0 kcal mol^{-1} ΔG value obtained from DFT calculations (see Theoretical Studies). Moreover, eq 3a has an extremely small equilibrium constant ($K_{3a} \cong 10^{-10}$), as derived from the redox potentials of $Pt_3(CO)_2I$ in Table 1. To this purpose, it is worth noting that disproportion reactions like eq 3a and analogous ones of the type $2L_nM^{n+} \leftrightarrows L_nM^{(n-1)+} + L_nM^{(n+1)+}$, in which the three species are identical except the charge, are generally endoergonic because the addition of one electron to a given system is comparatively less favored when the acceptor is less positive. In other words, for the processes $L_nM^{(n+1)+} + e^- \leftrightarrows L_nM^{n+} + e^- \leftrightarrows L_nM^{(n-1)+}$ it is usually observed that the former has a higher $E°$, which gives a negative value of $\Delta E°$ for the disproportionation reaction.[28] Accordingly, we may evaluate from the experimental redox potentials in Table 1 that the disproportions of the 43e$^-$ species $[Pt_3(CO)_3]^{2+}$, $[Pt_3(CO)_2I]^+$, $Pt_3(CO)I_2$ and $[Pt_3I_3]^-$ are all endoergonic, with a roughly constant energy cost ($\Delta G°$ = +9.9, +13.4, +12.2 and 12.0 kcal mol^{-1}, respectively). Conversely, disproportion of the metal oxidation state may take place when the environments of the two equal molecules are differently modified. As it will be further discussed in the Theoretical Studies, such a possibility may be achieved through alternative CO/I$^-$ substitutions at the 43e$^-$ intermediate $[Pt_3(CO)_2I]^+$. For example, the excess of I$^-$ may favor the sequential formation of the 43e$^-$ derivatives $[Pt_3(CO)I_2]$ and $[Pt_3I_3]^-$ (eqs 4a and 4b), while the CO molecules released in solution may lead to $[Pt_3(CO)_3]^{2+}$ (eq 4c). Given that up to four different 43e$^-$ species might exist in solution, various redox couples are possible, some of which have the proper potential for the exchange of one electron. Certainly, the best couple corresponds to the reactants in eq 4d, namely, $[Pt_3I_3]^-$ and $[Pt_3(CO)_3]^{2+}$, due to the largest difference ($\Delta E°$ = +1.85 V) between the corresponding redox potentials (−0.72 V and +1.13 V, respectively, in Table 1). As a further attractiveness of the mechanism proposed in eqs 4a−d, the 42e$^-$ and 44e$^-$ products Pt_3I_3 and $[Pt_3(CO)_3]^+$, formed in 1:1 mixture in the early steps of the reaction, are simultaneously formed in eq 4d.

$$\begin{array}{ll} \text{a)} & [Pt_3(CO)_2I]^+ + I^- \leftrightarrows [Pt_3(CO)I_2] + CO \\ \text{b)} & [Pt_3(CO)I_2] + I^- \leftrightarrows [Pt_3I_3]^- + CO \\ \text{c)} & [Pt_3(CO)_2I]^+ + CO \leftrightarrows [Pt_3(CO)_3]^{2+} + I^- \\ \text{d)} & [Pt_3(CO)_3]^{2+} + [Pt_3I_3]^- \leftrightarrows [Pt_3(CO)_3]^+ + Pt_3I_3 \end{array} \quad (4)$$

$$2\,[Pt_3(CO)_2I]^+ + I^- \leftrightarrows [Pt_3(CO)_3]^+ + Pt_3I_3 + CO$$

Since, except for $[Pt_3(CO)_2I]^+$, there is no experimental evidence for any of the other possible 43e$^-$ intermediates, systematic DFT studies were carried out. The purpose of the latter was to evaluate the stability of the various possible minima and construct an overall potential energy surface (PES) to shed light on the most favorable succession of events.

2.5. Theoretical Studies. To gain an overview of the TPCs of importance in this paper, DFT calculations were carried out for clusters with all the possible combinations of terminal CO and I$^-$ ligands and having VEC values in the range 44−42. The functional used was B3LYP[29] with the LANL2DZ basis set,[30] and the approach included the conductor-like polarizable continuum model (CPCM) for the dichloromethane solvent.[31] As previously observed,[19c] the usage of the solvent is fundamental to compare differently charged units. The phosphorus bridges were treated as real PBu^t_2 groups in order to avoid major energy biases and possible underestimation of the steric effects. In summary we optimized twelve species of generalized formula $\{Pt_3(CO)_nI_{3-n}\}^{x-n}$, n = 0 → 3, x = 1 → 3, in which the curly brackets help to distinguish computed models from the experimental species.

2.5.1. Structural Aspects of Optimized Structures. We first focus on $\{Pt_3I_3\}$, which is the ultimate and unprecedented product of this chemistry. The agreement with the experimental Pt_3I_3 structure of Figure 3 is satisfactory, its symmetry being almost D_{3h}. The computed Pt−Pt distances are somewhat longer than the experimental ones (2.68 Å vs 2.59 Å), but still correspond to single bonds. The effect is likely due to the pseudopotential used for the Pt atoms,[32] reflected also by a similar ∼0.1 Å overestimation of the Pt−P distances. The Pt−I distances are closer to the experimental ones (near 2.62 Å),

dx.doi.org/10.1021/ic400251y | Inorg. Chem. 2013, 52, 4635−4647

Table 3. Geometry Parameters of the Twelve Optimized Species in the 44−42e⁻ Redox Triads with General Formula $\{Pt_3(CO)_nI_{3-n}\}^{x-n}$, $n = 0 \rightarrow 3$, $x = 1 \rightarrow 3$[a]

	VEC	L_{1-3}	Pt_1-Pt_2	Pt_1-Pt_3	Pt_2-Pt_3	Pt_1-P_1	Pt_2-P_1	Pt_2-P_3	Pt−I	Pt−(CO)
$\{Pt_3(CO)_3\}^+$	44	$(CO)_3$	3.10	3.10	3.10	2.37	2.37	2.37		1.87
$\{Pt_3(CO)_3\}^{2+}$	43	$(CO)_3$	2.89	2.89	2.89	2.39	2.39	2.40		1.89
$\{Pt_3(CO)_3\}^{3+}$	42	$(CO)_3$	2.73	2.74	2.75	2.41	2.41	2.40		1.93
$\{Pt_3(CO)_2I\}$	44	$I(CO)_2$	2.95	2.94	3.34	2.36	2.34	2.40	2.62	1.86
$\{Pt_3(CO)_2I\}^+$	43	$I(CO)_2$	2.80	2.80	2.97	2.34	2.41	2.39	2.59	1.89
$\{Pt_3(CO)_2I\}^{2+}$	42	$I(CO)_2$	2.67	2.67	2.81	2.32	2.50	2.37	2.60	1.92
$\{Pt_3(CO)I_2\}^-$	44	$I_2(CO)$	3.11	3.11	3.01	2.39	2.36	2.34	2.60	1.85
$\{Pt_3(CO)I_2\}$	43	$I_2(CO)$	2.86	2.86	2.77	2.41	2.34	2.36	2.62	1.87
$\{Pt_3(CO)I_2\}^+$	42	$I_2(CO)$	2.75	2.74	2.65	2.43	2.32	2.38	2.64	1.89
$\{Pt_3I_3\}^{2-}$	44	I_3	3.08	3.08	3.09	2.35	2.35	2.36	2.60	
$\{Pt_3I_3\}^-$	43	I_3	2.84	2.83	2.84	2.36	2.36	2.36	2.62	
$\{Pt_3I_3\}$	42	I_3	2.68	2.68	2.68	2.36	2.36	2.36	2.63	

[a]In compounds with mixed terminal ligands, Pt_1 is the atom bound to the unique CO or I^- ligand.

possibly because the pseudopotential, used also for the iodine atoms, compensates the effects. Table 3 compares the most important geometric variations for the twelve TPCs $\{Pt_3(CO)_{3-n}I_n\}^{x-n}$, $n = 0 \rightarrow 3$, $x = 1 \rightarrow 3$. The equilateral Pt_3 triangle in the symmetric 44e⁻ models $\{Pt_3(CO)_3\}^+$ and $\{Pt_3I_3\}^{2-}$ is similarly expanded with respect to the 42e⁻ derivatives $\{Pt_3(CO)_3\}^{3+}$ and $\{Pt_3I_3\}$. The ∼0.4 Å difference in Pt−Pt linkages implies the change of the bond order from 1 to 0.66.[26] The geometry of $\{Pt_3(CO)_3\}^+$ is consistent with that observed in $[Pt_3(CO)_3]CF_3SO_3$,[11g] disregarding the ∼0.1 Å overestimation of the Pt−Pt distances (3.10 vs 2.99 Å). Moreover, the isolectronic $\{Pt_3I_3\}^{2-}$ analogue (not experimentally available) is found to be quite similar (Pt−Pt = 3.08 Å), hence the simple substitution of terminal ligands does not seem to be crucial for the geometry of the Pt_3 core. The Pt−I distances (2.613 Å, average) are similar in all the I-containing models. For TPCs with mixed terminal ligands, as in the series starting with $\{Pt_3(CO)_2I\}$ or $\{Pt_3(CO)I_2\}^-$, the Pt_3 triangle is isosceles.

No X-ray structure of any iodo-carbonyl derivative is available, but the known analogue $Pt_3(\mu\text{-}PBu^t_2)_3(CO)_2Cl$[19a] confirms that the Pt−Pt vector opposite to the halide ligand is more elongated (3.152 vs 2.855 Å) as found in our model $\{Pt_3(CO)_2I\}$ (3.34 vs 2.94 Å). Inverse shortening is instead observed for the Pt−Pt vector opposite to CO (3.01 vs 3.11 Å) in $\{Pt_3(CO)I_2\}^-$. On the other hand, it is known that the nature of one terminal ligand affects the opposite Pt−Pt interaction up to its cleavage in some extreme case, such as $Pt_3(\mu\text{-}PBu^t_2)_3(CO)_2H$.[19b] A general electronic analysis of the latter phenomenon, also known as cluster-core (or Pt−Pt bond) stretching isomerism,[33,20] will be presented elsewhere.

The MO scheme of Figure 4 for a D_{3h} TPC helps to understand the geometric trends imposed by the electron population.[26] The Pt_3 σ bonding framework is formed by radial and tangential d orbitals, which form three lower bonding levels (all populated) and three higher σ^* ones. One of the latter, a_2', lies in the frontier region and is vacant for VEC = 42, consistently with three single Pt−Pt bonds. Two more electrons in the level reduce the equivalent bond order to 0.66.

The a_2' level (Figure 4a) is not purely metallic, but has a significant contribution from the in-plane phosphido p orbitals, which mix in a bonding way to the metals (Figure 4b). Thus, the electrons in a_2' reduce the Pt−P distances, as confirmed by comparing the various redox series in Table 3. Although the effect is not large (maximum difference of ∼0.04 Å), the D_{3h}

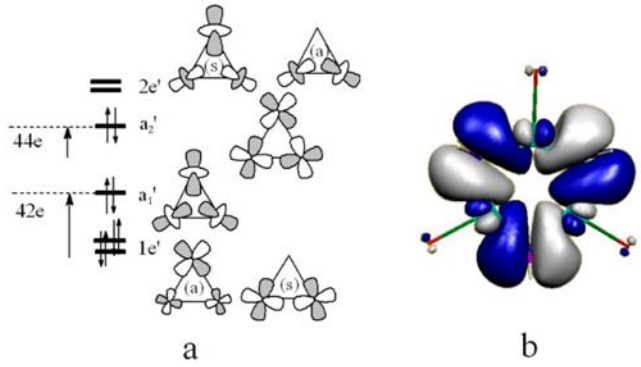

Figure 4. (a) Basic aspects of the Pt_3 frontier MOs, populated up to a_2' for VEC = 44; (b) DFT generated drawing of the a_2' wave function.

TPCs with only CO or I^- terminal ligands have shorter Pt−P bond lengths in electron richer species.[34]

2.5.2. Energy Profiles. As anticipated, a concerted process leading to the 42e⁻ species $\{Pt_3I_3\}$ by direct reaction between $\{Pt_3(CO)_2I\}$ and I_2 (path a in Scheme 1) was reasonably discarded in spite of the about −50 kcal mol^{-1} energy gain, as determined from optimized components (see Supporting Information). It is instead more probable that different TPCs may be formed upon sequential substitution/redox steps. Therefore, all the possible species (including the experimentally undetected $\{Pt_3(CO)I_2\}^n$ series) were optimized and are outlined in Scheme 3, together with all the free energy variations, ΔG. For the redox steps, also the corresponding values, ΔG°_{redox}, obtained through the Nernst equation[35] from the experimental or extrapolated redox potentials, are given in italics (see Table 1 and the Experimental Section).

It is found that the equation $\Delta G^\circ_{redox}(exp) = 0.86(7)\ \Delta G_{redox}(calc) - 13(8)$ kcal mol^{-1} correlates computed and experimental ΔG values for the various redox steps. The agreement appears satisfactory in view of the correlation coefficient ($R = 0.99$) and the small probability factor ($P < 1.0 \times 10^{-4}$),[25] as also confirmed by the plot in Figure 5. The most ill-behaved species are those with the highest molecular charges, likely because the counterions were neglected in the calculations. For instance, the oxidation to $[Pt_3(CO)_3]^{3+}$ is computed to cost +10.2 kcal mol^{-1} more than in the experiment, while that of $[Pt_3I_3]^{2-}$ is underestimated by 4.5 kcal mol^{-1}. By neglecting the latter two points, the correlation is expressed by the equation $\Delta G^\circ_{redox}(exp) = 1.0\ (1)$-

dx.doi.org/10.1021/ic400251y | Inorg. Chem. 2013, 52, 4635−4647

Scheme 3. Free Energy Map (kcal mol^{-1}) of All the Possible Redox/Substitution Steps ($[Pt_3(CO)_nI_{3-n}]^{x-n}$, $n = 0 \rightarrow 3$, $x = 1 \rightarrow 3$)[a]

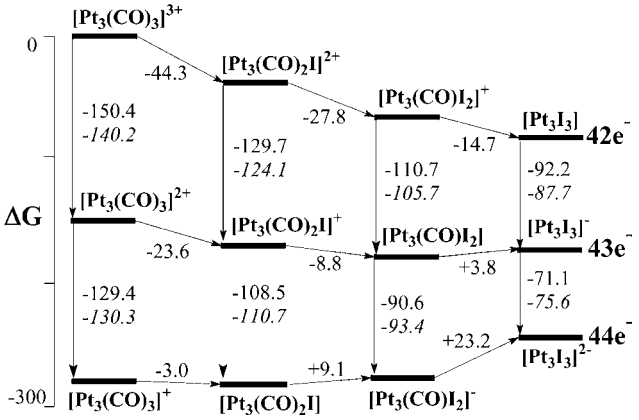

[a]The ΔG°_{redox} values, from experimental potentials, are in italics.

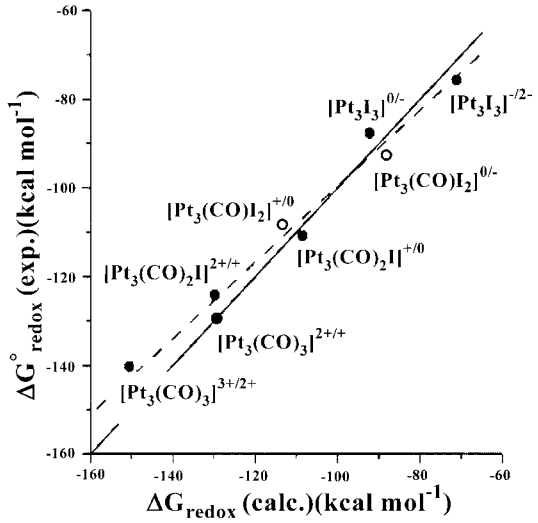

Figure 5. Correlation (dashed line) between the calculated and the experimental ΔG_{redox} values for all the one electron reduction in the series $[Pt_3(CO)_3]^+$, $Pt_3(CO)_2I$, $[Pt_3(CO)I_2]^-$ (extrapolated with empty circles) and $[Pt_3I_3]^{2-}$. The solid line corresponds to the ideal match between calculated and experimentally based ΔG_{redox} values.

ΔG_{redox}(calc) − 4(18) kcal mol^{-1} and the dashed and solid lines of Figure 5 become almost superimposed.

Incidentally, the Nernst equation[35] permits derivation of redox potentials from the computed ΔG value for each redox step, giving E°_{calc} values that compare satisfactorily with the experimental ones (see Table S1 in the Supporting Information). As confirmed by Scheme 3, the computed costs of the 43e$^-$/42e$^-$ oxidations are progressively overestimated for the increasing number of CO ligands, while the corresponding 43e$^-$/44e$^-$ reductions are less underestimated. The two effects sum up in the disproportion of any 43e$^-$ species, so that the computed process appears more endoergonic (∼+21 kcal mol^{-1}, average) than in the experiment (∼+12 kcal mol^{-1}, average). In spite of the latter difference, the general trends seem fully validated. Thus, the addition of one electron to any TPC naturally lowers the total energy, but the 43e$^-$/44e$^-$ transformation is less exoergonic than the corresponding 42e$^-$/43e$^-$. An explanation is that the energy of the frontier a_2' level (Figure 4) depends on its electron population (SOMO < LUMO) being strictly related to the charge of the system (for instance, more iodide ligands reduce the positive charge of the Pt_3 unit).

For similar reasons, the formation of any 44e$^-$ species is comparatively more difficult than that of its 43e$^-$ precursor, since the framework has one less positive charge hole. Concerning the general substitution trends, one uncharged CO ligand in place of an iodide is exoergonic when occurring at a positively charged Pt_3 framework, but endoergonic for an uncharged or anionic one. Again, the electrostatic factors play an important role over the entire mechanistic profile. In addition, the replacement of one CO with an I$^-$ ligand is easier at a less electron rich species (lower VEC), since metal−CO back-donation is already less effective (calculated CO-stretchings are reported in Table S2 in the Supporting Information). The entire process starts with $\{Pt_3(CO)_2I\}$ which is easily oxidized by I_2. Such experimental evidence is validated by the DFT calculations, since the energy balance of the corresponding eq 5 is as negative as −28.6 kcal mol^{-1} (the single energy components are provided in the Supporting Information). In contrast, a second oxidation of $\{Pt_3(CO)_2I\}$ by I_2 to give $\{Pt_3(CO)_2I\}^{2+}$ (discarded in terms of redox potentials) is endoergonic by +13.7 kcal mol^{-1}.

$$2\{Pt_3(CO)_2I\} + I_2 \rightarrow 2\{Pt_3(CO)_2I\}^+ + 2I^- \quad (5)$$

As already remarked from the experimental findings, the 43e$^-$ derivative $\{Pt_3(CO)_2I\}^+$ is the key intermediate, which, after alternative terminal ligand substitutions, might generate the appropriate redox couple able to give the 42e$^-$ and 44e$^-$ coproducts $\{Pt_3I_3\}$ and $\{Pt_3(CO)_3\}^+$. In the iodide rich environment, the $\{Pt_3(CO)I_2\}$ and $\{Pt_3I_3\}^-$ species can be subsequently formed, and, according to Figure 2 and Scheme 3, they are more prone to be oxidized to the corresponding 42e$^-$ derivatives. The substitution to give $\{Pt_3(CO)I_2\}$ is exoergonic (—8.8 kcal mol^{-1}), while that leading to $\{Pt_3I_3\}^-$ is slightly endoergonic (+3.8 kcal mol^{-1}). In contrast, the formation of $\{Pt_3(CO)_3\}^{2+}$, as a potential redox partner (eq 4c), costs as much as +23.6 kcal mol^{-1}, although such a barrier may be partially avoided (see section 2.5.3). The costly substitution steps are eventually compensated by the significantly exoergonic redox reaction between $\{Pt_3(CO)_3\}^{2+}$ and $\{Pt_3I_3\}^-$ (−37.2 kcal mol^{-1}). The corresponding ΔG° value, derived from the experimental potentials in Table 1, is not very different (−42.6 kcal mol^{-1}).

A more general problem, concerning the redox reaction between two different 43e$^-$ TPCs, is that the single electron to be transferred lies in the inner frontier a_2' level having Pt_3 σ^* character (see Figure 4). This implies that the MOs of the two molecules, which exchange the electron, are not reciprocally directional and their overlap is practically null, even if the molecules lie relatively close to each other. In this respect, consider that the nature of the substitution reactions, pointed out up to now, have not been examined in terms of their potential associative/dissociative character. Depending on the latter, the geometric and electronic features of the 43e$^-$ planar clusters (in particular the SOMO) can be momentarily perturbed. The problem is analyzed in the section 2.5.3.

2.5.3. Associative Intermediates in the Terminal Ligand Substitution Reactions. A dissociative mechanism can be reasonably dismissed in view of the about +26.0 kcal mol^{-1} energy cost for detaching one CO ligand from the 43e$^-$ species $\{Pt_3(CO)_2I\}^+$ to form $\{Pt_3(CO)I\}^+$ (its optimized 41e$^-$

dx.doi.org/10.1021/ic400251y | Inorg. Chem. 2013, 52, 4635−4647

minimum is presented in the Supporting Information). Conversely, 45e$^-$ associative intermediates (not transition states!) are exoergonically formed as shown, for instance, by $\{Pt_3(CO)_2I_2\}$, which gains −5.1 kcal mol^{-1}. The latter species, shown in Figure 6a, has a perpendicular iodide ligand over one

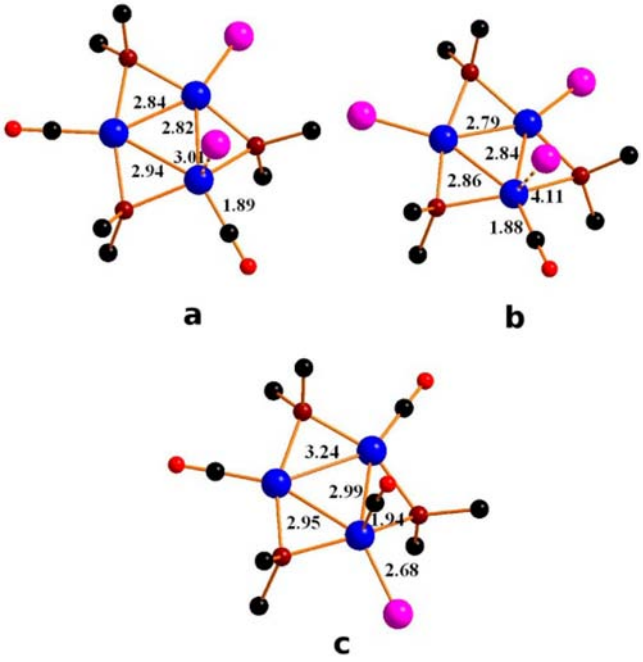

Figure 6. Optimized structures of the 45e$^-$ adducts: (a) $Pt_3(\mu\text{-}PBu^t_2)_3(CO)_2I_2$, $\{Pt_3(CO)_2I_2\}$; (b) $[Pt_3(\mu\text{-}PBu^t_2)_3(CO)I_3]^-$, $\{Pt_3(CO)I_3\}^-$; (c) $[Pt_3(\mu\text{-}PBu^t_2)_3(CO)_3I]^+$, $\{Pt_3(CO)_3I\}^+$.

CO-coordinated Pt atom (Pt−I = 3.01 Å), but the approached tetra-coordination induces only minor geometric (hence electronic) perturbations at the underlying Pt_3 framework. In fact, the Pt−Pt distances remain essentially unchanged and only a minor out-of-plane bending of the phosphido bridges is observed.

More interesting are the other two possible 45e$^-$ adducts preceding $\{Pt_3I_3\}^-$ and $\{Pt_3(CO)_3\}^{2+}$, which in principle constitute a well-suited redox couple to form the 1:1 mixture of $\{Pt_3I_3\}$ and $\{Pt_3(CO)_3\}^+$ (eq 4d). The geometry of the $Pt_3(\mu\text{-}PR_2)_3$ core in $\{Pt_3(CO)I_3\}^-$ (Figure 6b) is essentially unperturbed (the new Pt−I distance being as long as 4.11 Å), but the adduct is still somewhat stabilized (—2.3 kcal mol^{-1}) with respect to the substituted species $\{Pt_3I_3\}^-$. In the two examined 45e$^-$ intermediates, the basic electronic picture does not change, as the SOMO maintains the original a_2' character highlighted in Figure 4. The situation is instead different for $\{Pt_3(CO)_3I\}^+$ (Figure 6c), where one CO ligand has attacked the key 43e$^-$ species $\{Pt_3(CO)_2I\}^+$.

The newly formed and perpendicular Pt−CO bond is rather strong (1.94 Å) and affects the nature of the SOMO. The latter, which is shown in Figure 7, clearly indicates that the unpaired electron occupies a perpendicularly hybridized z^2 orbital *trans* to the entering CO.

At the same time, the a_2' Pt_3 σ^* level has to be fully populated with a generalized expansion of the Pt_3 triangle (Figure 6c) similarly to 44e$^-$ species. Because of its outpointing metal lobe, the new SOMO seems particularly suited to favor the electron transfer from another 43e$^-$ TPC, such as $\{Pt_3(CO)I_2\}$ or $\{Pt_3I_3\}^-$, although the 45e$^-$ adduct $\{Pt_3(CO)$-

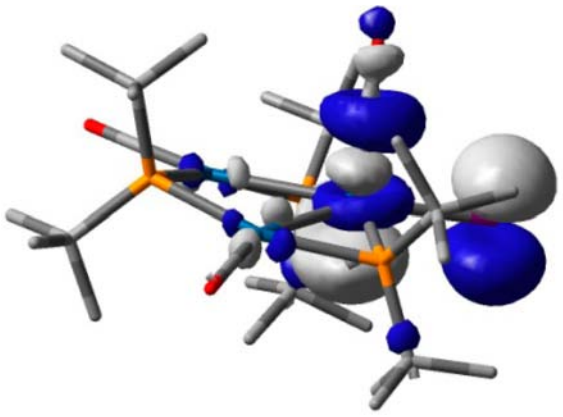

Figure 7. SOMO of the adduct $[Pt_3(\mu\text{-}PBu^t_2)_3(CO)_3I]^+$, $\{Pt_3(CO)_3I\}^+$.

$I_3\}^-$ of Figure 6b is a better candidate for having a similarly featured SOMO. In spite of the +12.7 kcal mol^{-1} destabilization of $\{Pt_3(CO)_3I\}^+$ with respect to the reactants $\{Pt_3(CO)_2I\}^+$ + CO, the direct participation of the adduct in the redox process avoids the much more expensive attainment of $\{Pt_3(CO)_3\}^{2+}$ (+23.6 kcal mol^{-1}), otherwise considered to be the most immediate precursor of the coproduct $\{Pt_3(CO)_3\}^+$.

Based on the DFT calculations, the probable steps can be monitored with the help of Scheme 4. At the top, the initial

Scheme 4. Proposed Steps of the Reaction Mechanism Triggered by I_2

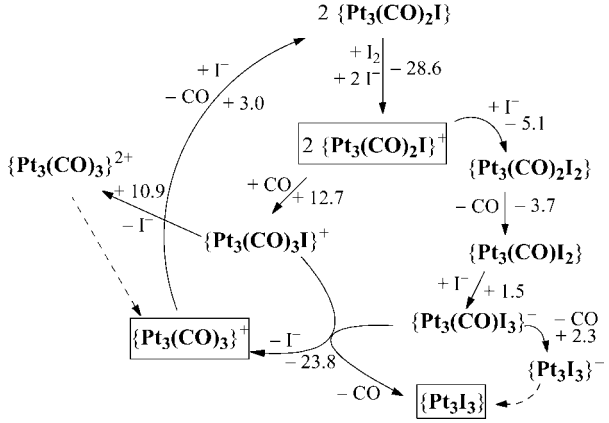

monoelectronic oxidation of $\{Pt_3(CO)_2I\}$ by I_2 exoergonically leads to the formation of the key 43e$^-$ intermediate $\{Pt_3(CO)_2I\}^+$ and free iodide anions. Subsequent substitution reactions are fundamental to create different 43e$^-$ derivatives with redox potentials suitable to one electron transfer. Initially, the null concentration of free CO excludes any left side route in Scheme 4. At the right side, one iodide can attack $\{Pt_3(CO)_2I\}^+$, allowing sequential exoergonic formations of the adduct $\{Pt_3(CO)_2I_2\}$ and of the substitution product $\{Pt_3(CO)I_2\}$. The attack of a second iodide ligand to form $\{Pt_3(CO)I_3\}^-$ and eventually $\{Pt_3I_3\}^-$ is similar but has some small energy cost.

Upon the substitution with iodides, the higher concentration of free CO in solution might allow the potential formation of $\{Pt_3(CO)_3I\}^+$ and $\{Pt_3(CO)_3\}^{2+}$ in a sequence (left side of Scheme 4). The processes are both destabilizing, but the former adduct requires only about half energy compared to the latter

dx.doi.org/10.1021/ic400251y | *Inorg. Chem.* 2013, 52, 4635−4647

substitution product. Therefore, also in view of its orbital features (Figure 7), $\{Pt_3(CO)_3I\}^+$ may represent the proper redox partner (bottom of Scheme 4) of either $\{Pt_3I_3\}^-$ or $\{Pt_3(CO)I_3\}^-$ (the fact that both the 45e$^-$ species are minima, rather than transition states, suggests that their lifetime may be sufficient for their reaction to occur with an energy gain of −23.8 kcal mol^{-1}). Finally, Scheme 4 reminds that the coproduct $\{Pt_3(CO)_3\}^+$ slowly converts into the 44e$^-$ precursor $\{Pt_3(CO)_2I\}$, which can reenter in circle and react with I_2, till $\{Pt_3I_3\}$ is quantitatively formed.[36]

2.5.4. The Role of Terminal Halides in Favoring 42e$^-$ vs 44e$^-$ TPCs. Since the tris-phosphido-bridged TPCs known up to now have 44 valence electrons, we look for an explanation of the unique role played by the terminal halides. A first intuitive answer is the unbearable concentration of negative charges in the hypothetical 44e$^-$ dianions $[Pt_3(\mu\text{-}PR_2)_3X_3]^{2-}$, where significant electron repulsions are already implicit in the Pt_3 σ^* character of the HOMO a_2' (Figure 4). Terminal ligands with π-acceptor character limit through back-donation the accumulation of electron density at the metals, while π-donor halides have the opposite effect. The diagram of Figure 8a shows how the HOMO is the product of a classical three-orbital interaction, which involves the filled combination of the phosphido p orbitals (right side) and both those formed by the metal d_π and p_π ones (left side). The latter is the acceptor of the phosphido electrons allowing one of the six Pt−P delocalized bonds. However, the corresponding a_2' MO also combines with the corresponding filled combination of the d_π orbitals, which is Pt−Pt antibonding by nature and raises the energy of the HOMO.

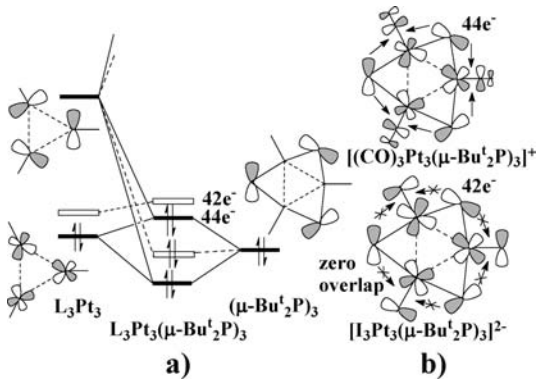

Figure 8. (a) Different perturbation theory effects on the two frontier levels of a_2' type in 44e$^-$ (black bars) and 42e$^-$ (white bars) TPCs. (b) Comparison of the higher a_2' MO in presence of π-acceptor (upper drawing) or π-donor (lower drawing) terminal ligands.

According to perturbation theory,[37] the d_π/p_π rehybridization prevents a too high a_2' destabilization but, in this respect, the π features of the terminal ligands determine a crucial difference (Figure 8b). In fact, three π-donor halides, antibonding toward the metal d_π orbitals, are already destabilizing for the HOMO, which is prone to convert into the LUMO of 42e$^-$ species (higher white bar in Figure 8a). This implies removal of the Pt−Pt σ^* electrons, hence shorter Pt−Pt distances.

The CO vs iodide ligands also peculiarly affects the nature of the a_2' level in question (Figures 8b). While the CO π^* levels (upper drawing) positively overlap with the metal d_π ones (as well as with the p_π bridges), the corresponding combination of the halides is antibonding with the d_π one, forcing the p_π bridges to fall on the nodal surfaces across the Pt−X linkages (lower drawing). The practically null overlap does not allow the favorable perturbation theory effect, which for 44e$^-$ species reduces the HOMO destabilization. For this reason, $\{Pt_3I_3\}^{2-}$ and its congeners are undetected as the 42e$^-$ count is preferred. Therefore, the two highest MOs (empty bars of Figure 8a) are essentially contributed from Pt_3 d_π and P_3 p_π orbitals.

Similarly based arguments likely account for the experimentally observed order of stability Pt_3I_3 > Pt_3Br_3 > Pt_3Cl_3. Without going into deep orbital details, but referring to the qualitative lower drawing of Figure 8b, it may be deduced that the nodal surfaces perpendicular to the Pt−X vectors may be somewhat shifted depending on the diffusion and energy (electronegativity) of the various halide p_π orbitals, thus affecting the critical $\langle P_3|Pt_3X_3\rangle$ overlap. Only for three iodides, the latter is practically null, hence the system has more propensity than the others to be most stable in the 42e$^-$ configuration.

3. CONCLUSIONS

This paper has presented the synthesis and full characterization of the first examples of tris-phosphido-bridged clusters with 42 rather than the typical 44 valence electrons. This is possible only with three terminal halides and we have focused in particular on the formation of the best characterized Pt_3I_3 species. The latter has been prepared by an initial chemical (I_2 oxidant) or electrochemical monoelectronic oxidation of the 44e$^-$ precursor $Pt_3(CO)_2I$, which affords the paramagnetic 43e$^-$ intermediate $[Pt_3(CO)_2I]^+$.

This undergoes ligand substitution processes with the formation of two different 43e$^-$ frameworks, which can exoergonically exchange one electron. The formation of the latter redox couple is important to understand how a 42e$^-$ product may be reached, since both chemical and electrochemical evidence exclude that the I_2 oxidant can perform a second monoelectronic oxidation. A single electron transfer instead occurs between two 43e$^-$ TPCs to produce an equimolar mixture of $[Pt_3(CO)_3]^+$ and Pt_3I_3. The reaction continues with a new transformation of $[Pt_3(CO)_3]^+$ into $[Pt_3(CO)_2I]^+$ due to the simultaneous presence of I_2 and I^- till Pt_3I_3 is quantitatively formed. The DFT calculations have been a precious tool to characterize all the intermediates which may be formed in solution (many of them experimentally undetected). All the species have been of importance to map the overall energy profile for the series of substitution and redox reactions and their relative sequence. Also, it has been computationally proved that some 45e$^-$ associative intermediates with one tetra-coordinated Pt atom help smooth some unfavorable energy cost along the entire pathway, which in particular precede the well characterized $Pt_3I_3/[Pt_3(CO)_3]^+$ 1:1 mixture. Finally, some MO argument has been presented to justify the role of the halides in stabilizing the unique 42e$^-$ TPCs with three phosphido bridges, also with some hint on the increasing stability in the order Pt_3I_3 > Pt_3Br_3 > Pt_3Cl_3.

4. EXPERIMENTAL SECTION

4.1. General Data. The reactions were carried out under a nitrogen atmosphere, by using standard Schlenk techniques. $Pt_3(\mu\text{-}PBu^t_2)_3(CO)_2X$ (X = Cl, Br, I) were prepared as previously described.[11a,b,19a] Solvents were dried by conventional methods and distilled under nitrogen prior to use. NMR spectra were recorded on a Varian Gemini 200 BB instrument (200 MHz for ^{1}H) at room temperature (about 293 K) on $CDCl_3$ solutions; frequencies are

dx.doi.org/10.1021/ic400251y | Inorg. Chem. 2013, 52, 4635−4647

referenced to the residual resonances of the deuterated solvent (H, ^{13}C), to 85% H_3PO_4 (^{31}P), and to H_2PtCl_6 (^{195}Pt).

4.2. Electrochemistry. Electrochemical measurements were performed in 0.2 M dichloromethane solutions of [^{n}Bu$_4$N]PF_6 or [^{n}Bu$_4$N]X (X = Cl, Br, I) as supporting electrolyte. HPLC grade dichloromethane (Sigma-Aldrich) was stored under nitrogen over 3 Å molecular sieves. [^{n}Bu$_4$N]PF_6 (Fluka, electrochemical grade), [^{n}Bu$_4$N]I (Fluka, electrochemical grade), [^{n}Bu$_4$N]Cl (Fluka, puriss. p.a.) and [^{n}Bu$_4$N]Br (Fluka, electrochemical grade) were used as purchased. Cyclic voltammetry was performed in a three-electrode cell having a platinum working electrode surrounded by a platinum-spiral counter electrode and the aqueous saturated calomel reference electrode (SCE) mounted with a Luggin capillary, and containing a 5×10^{-4} M analyte solution. A BAS 100W electrochemical analyzer was used as a polarizing unit. Hydrodynamic voltammetry made use of a platinum electrode with periodical renewal of the diffusion layer, obtained by moving the solid electrode with a time-controlled knocker. Controlled potential coulometry was performed in an H-shaped cell with anodic and cathodic compartments separated by a sintered-glass disk. The working macroelectrode was a platinum gauze; a mercury pool or a platinum grid was used as the counter electrode. All reported potential values are referred to the saturated calomel electrode (SCE). Under the experimental conditions, the one-electron oxidation of ferrocene occurs at $E^{\circ\prime}$ = +0.39 V. Free energy values, ΔG°_{redox}, were obtained from the potentials $E^\circ_{(CH2Cl2)}{}^{abs}$ through application of the Nernst equation ($\Delta G^\circ_{redox} = -FE^\circ_{(CH2Cl2)}{}^{abs}$, where F is the Faraday constant = 23.06 kcal mol^{-1} V^{-1}),[35] In actuality, $E^\circ_{(CH2Cl2)}{}^{abs}$ corresponds to the following combination:

$$E^\circ_{(CH2Cl2)}{}^{abs} = E^\circ_{(CH2Cl2)}{}^{SCE} + E^\circ_{(SCE,aq)}{}^{abs} - E_L \qquad (6)$$

where $E^\circ_{(CH2Cl2)}{}^{SCE}$ is the value of the measured potential, $E^\circ_{(SCE,aq)}{}^{abs}$ is 4.522 V and E_L is the interliquid potential, which depends on the nature of the solvent as well as on the composition of the solution (nature and concentration of the electrolyte).[38] The exact amount of the latter is unknown, but it is expected to represent only a minor contribution,[38] therefore it has been omitted in the present estimation.

4.3. Synthesis of Pt_3I_3. A solution of I_2 (74 mg, 0.29 mmol) in 7 mL of CH_2Cl_2 was added to a solution of **$Pt_3(CO)_2I$** (350 mg, 0.29 mmol) in 15 mL of CH_2Cl_2. Immediately after mixing, the ^{31}P NMR spectrum of the solution showed the signals of **Pt_3I_3** and [**$Pt_3(CO)_3$**]$^+$ (in roughly 1:1 ratio) together with those of the reactant **$Pt_3(CO)_2I$.** The solution was stirred for 12 h at 25 °C. During this time the color of the solution changed from brown to violet. Removal of solvent afforded a violet solid. Further purification was accomplished by flash chromatography using silica gel and hexane as eluent. Removal of solvent *in vacuo* gave **Pt_3I_3** as a violet solid in 77% yield (313 mg). Violet single crystals of **Pt_3I_3** suitable for X-ray analysis were obtained by recrystallization from $CHCl_3$. ^{1}H NMR (200 MHz, $CDCl_3$, 25 °C): δ = 1.76 ppm (vt, ^3J(H,P) + ^5J(H,P) = 7.5 Hz). ^{13}C{^{1}H} NMR (50.3 MHz, $CDCl_3$, 25 °C): δ = 52.5 (C, Bu^t), 32.0 ppm (CH_3, Bu^t). ^{31}P{^{1}H} NMR (81.0 MHz, $CDCl_3$, 25 °C): δ = 405.3 ppm (s, ^2J(P,P) = 242 Hz, ^1J(P,Pt) = 1743 Hz, ^2J(P,Pt) = −22 Hz).[39] ^{195}Pt{^{1}H} NMR (42.8 MHz, $CDCl_3$, 25 °C): δ = −3684 ppm (m, ^1J(Pt,Pt) = 6434 Hz, ^1J(P,Pt) = 1743 Hz, ^2J(P,Pt) = −22 Hz).[39] Elemental analysis calcd (%) for $C_{24}H_{54}I_3P_3Pt_3$: C 20.57, H 3.88. Found: C 20.48, H 4.03.

4.4. Electrochemical Synthesis of [$Pt_3(CO)_2I$]$^+$ and Reaction with I$^-$. A solution of **$Pt_3(CO)_2I$** (4.8 mg, 4×10^{-3} mmol) in CH_2Cl_2 (7.0 mL) containing [^{n}Bu$_4$N]PF_6 0.2 M was electrolyzed at the first anodic step (E_w = +0.4 V). Upon the passage of 1 faraday per mole, the yellow solution became dark brown and the current dropped to a very small value. A cyclic voltammetry of the solution showed the quantitative formation of [**$Pt_3(CO)_2I$**]$^+$. On adding [^{n}Bu$_4$N]I (4.4 mg, 1.2×10^{-2} mmol) the solution changed color again and the reaction was monitored by cyclic voltammetry. In 15 min a pink solution was obtained showing two reduction processes at −0.72 and −1.29 V. The solution was concentrated to 0.5 mL and analyzed by ^{31}P NMR analysis, which confirmed the formation of **Pt_3I_3**.

4.5. Synthesis of Pt_3Br_3. A CH_2Cl_2 solution (5 mL) of Br_2 (6 μL, 0.12 mmol) was added to a solution of **$Pt_3(CO)_2Br$** (140 mg, 0.12 mmol) in 10 mL of CH_2Cl_2 cooled to −20 °C. The solution was stirred for 1 h at −20 °C and then for 6 h at room temperature. Removal of solvent afforded a pink solid. Further purification was accomplished by flash chromatography using silica gel and hexane as eluent. Removal of solvent *in vacuo* gave **Pt_3Br_3** as a pink solid in 74% yield (112 mg). Pink crystals suitable for the X-ray analysis of **Pt_3Br_3** were grown by recrystallization from $CHCl_3$. ^{1}H NMR (200 MHz, $CDCl_3$, 25 °C): δ = 1.64 ppm (^3J(H,P) + ^5J(H,P) = 7.7 Hz). ^{13}C{^{1}H} NMR (50.3 MHz, $CDCl_3$, 25 °C): δ = 51.3 (C, Bu^t), 30.5 ppm (CH_3, Bu^t).^{31}P{^{1}H} NMR (81.0 MHz, $CDCl_3$, 25 °C): δ = 403.9 ppm (s, ^2J(P,P) = 240 Hz, ^1J(P,Pt) = 1725 Hz, ^2J(P,Pt) = −18 Hz).[39] ^{195}Pt{^{1}H} NMR (42.8 MHz, $CDCl_3$, 25 °C): δ = −3401 ppm (m, ^1J(Pt,Pt) = 6650 Hz, ^1J(P,Pt) = 1725 Hz, ^2J(P,Pt) = −18 Hz).[39] Elemental analysis calcd (%) for $C_{24}H_{54}Br_3P_3Pt_3$: C 22.87, H 4.32. Found: C 22.68, H, 4.23.

4.6. Electrochemical Synthesis of Pt_3Br_3. A solution of **$Pt_3(CO)_2Br$** (48 mg, 0.041 mmol) in CH_2Cl_2 (10 mL) with 0.2 M [^{n}Bu$_4$N][Br] was electrolyzed at the first anodic step (E_w = +0.4 V). When 2 faradays per mole had passed, the current level had decreased to a very small value. At this point, the electrolysis was considered to be complete and the reaction was stopped. Upon the addition of petroleum ether to the pink solution obtained, an oil separated out. The oil was washed twice with petroleum ether and the extracts were evaporated to dryness. The red residue was purified by column chromatography using silica gel and acetone, then hexane and finally dichloromethane as eluents. Removal of the solvent *in vacuo* gave **Pt_3Br_3** as a microcrystalline pink solid (38 mg, 0.03 mmol, 73% yield).

4.7. Synthesis of Pt_3Cl_3. The compound **$Pt_3(CO)_2Cl$** (80 mg, 72 mmol) was dissolved in CH_2Cl_2 (5 mL) and cooled to −40 °C. PCl_5 (15 mg, 72 mmol) was added and the solution was stirred for 3 h at −40 °C. The solution was then allowed to warm to room temperature. All the volatiles were removed *in vacuo*, and the residue was washed with acetone and was passed over a silica gel chromatographic column (acetone, then hexane and finally dichloromethane as eluents). Removal of the solvents *in vacuo* gave **Pt_3Cl_3** as a microcrystalline yellow solid (9 mg, 11% yield). Yellow crystals suitable for X-ray analysis of **Pt_3Cl_3** were grown by recrystallization from CH_2Cl_2. Anal. Calcd for $C_{24}H_{54}Cl_3P_3Pt_3$: C, 25.57; H, 4.83. Found: C, 25.43; H, 4.69. ^{1}H NMR (200 MHz, $CDCl_3$, 25 °C): δ = 1.59 ppm (^3J(H,P) + ^5J(H,P) = 7.5 Hz). ^{13}C{^{1}H} NMR (50.3 MHz, $CDCl_3$, 25 °C): δ = 50.9 (C, Bu^t), 30.0 ppm (CH_3, Bu^t). ^{31}P{^{1}H} NMR (81.0 MHz, $CDCl_3$, 25 °C): δ = 398.5 ppm (s, ^2J(P,P) = 240 Hz, ^1J(P,Pt) = 1736 Hz, ^2J(P,Pt) = −22 Hz).[39] ^{195}Pt{^{1}H} NMR (42.8 MHz, $CDCl_3$, 25 °C): δ = −3157 ppm (m, ^1J(Pt,Pt) = 6720 Hz, ^1J(P,Pt) = 1736 Hz, ^2J(P,Pt) = −22 Hz).[39] Elemental analysis calcd (%) for $C_{24}H_{54}Cl_3P_3Pt_3$: C 25.57, H, 4.83. Found: C 25.43, H 4.69.

4.8. Synthesis of [$Pt_3(CO)_2I$]PF_6. [Cp_2Fe]PF_6 (15 mg, 0.045 mmol) was added to a brown CH_2Cl_2 (3 mL) solution of **$Pt_3(CO)_2I$** (52 mg, 0.043 mmol) with stirring. After 30 min the solvent was removed in vacuo, the brown residue was washed with toluene and a brown-greenish solid was filtered off, vacuum-dried and identified as [**$Pt_3(CO)_2I$**]PF_6 (49 mg, yield 85%). Anal. Calcd for $C_{26}H_{54}F_6IO_2P_4Pt_3$: C, 23.15; H, 4.04. Found: C, 23.30; H, 4.09. IR: solid state, 2062 cm^{-1}; acetone solution, 2072 cm^{-1}. ^{1}H NMR (200 MHz, $CDCl_3$, 25 °C): δ (ppm) = 12.0 (br s, C*CH*$_3$). When we added a CH_2Cl_2 solution of Cp_2Co (0.05 M, 0.44 mL, 0.022 mmol) to a CH_2Cl_2 solution of [**$Pt_3(CO)_2I$**]PF_6 (30 mg, 0.022 mmol), the IR and ^{1}H and ^{31}P NMR spectra of the resulting solution exhibited only the signals of **$Pt_3(CO)_2I$** and [Cp_2Co]PF_6.

4.9. Reactivity of [$Pt_3(CO)_2I$]PF_6. *4.9.1. With [^{n}Bu$_4$N]I.* [^{n}Bu$_4$N]I (8 mg, 0.022 mmol) was added to an acetone (2 mL) solution of [**$Pt_3(CO)_2I$**]PF_6 (30 mg, 0.022 mmol). Immediately after mixing, the IR and the ^{31}P NMR spectra of the solution showed the signals of **Pt_3I_3** (δ_P = 404 ppm) and [**$Pt_3(CO)_3$**]$^+$ (ν_{CO} = 2072 cm^{-1}; δ_P = 151 ppm) (in rough 1:1 ratio). After addition of an excess of [^{n}Bu$_4$N]I (50 mg, 0.135 mmol) and stirring for 4 h the IR and ^{31}P NMR spectra showed the disappearance of the signals of the **$Pt_3(CO)_3$**$^+$ and the appearance of the signals of **$Pt_3(CO)_2I$** (ν_{CO} = 2025 cm^{-1}, δ_P = 171.8 and 64.6 ppm).

dx.doi.org/10.1021/ic400251y | *Inorg. Chem.* 2013, 52, 4635−4647

4.9.2. With [^{n}Bu$_4$N]I and I_2. [^{n}Bu$_4$N]I (8 mg, 0.022 mmol) and I_2 (3 mg, 0.012 mmol) were added to an acetone (2 mL) solution of $[Pt_3(CO)_2I]PF_6$ (30 mg, 0.022 mmol). After 2 h of stirring, the solution was concentrated to 0.5 mL and a ^{31}P NMR spectrum showed the presence of the signal of Pt_3I_3

4.10. Crystallography. Air stable crystals of Pt_3I_3, of Pt_3Br_3 and of Pt_3Cl_3 were mounted on a Bruker APEX II diffractometer for the unit cell, space group determination and data collection. Selected crystallographic and other relevant data are listed in Table 4 and in the Supporting Information. The space groups, unambiguously determined from the systematic absences, show that the three compounds are isomorphous. Data were corrected for Lorentz and polarization factors with the data reduction software SAINT[40] and empirically for absorption using the SADABS program.[41] The structures were solved by direct and Fourier methods and refined by full matrix least-squares[42] (the function minimized being $\sum[w(|F_o|^2 - (1/k)|F_c^2|)^2]$). The scattering factors used, corrected for the real and imaginary parts of the anomalous dispersion, were taken from the literature.[43] All calculations and plotting were carried out by using the PC version of SHELX-97,[42] WINGX, ORTEP[44] and Mercury programs.[45]

Table 4. Experimental Data for the X-ray Diffraction Study of Pt_3I_3, Pt_3Br_3 and Pt_3Cl_3

	Pt_3I_3	Pt_3Br_3	Pt_3Cl_3
formula	$C_{24}H_{54}I_3P_3Pt_3$	$C_{24}H_{54}Br_3P_3Pt_3$	$C_{24}H_{54}Cl_3P_3Pt_3$
mol wt	1401.55	1260.53	1127.19
data coll. T, K	295(2)	295(2)	295(2)
diffractometer	Bruker APEXII		
crystal size, mm	0.2 × 0.1 × 0.1	0.2 × 0.2 × 0.2	0.2 × 0.1 × 0.1
cryst syst	hexagonal	hexagonal	hexagonal
space group (no.)	$P6_3/m$ (176)	$P6_3/m$ (176)	$P6_3/m$ (176)
a, Å	12.455(1)	11.9553(8)	11.662(1)
V, Å^3	14.377(1)	14.656(1)	14.869(2)
Z	2	2	2
ρ_{calcd}, g cm^{-3}	2.410	2.308	2.137
μ, cm^{-1}	133.72	149.87	123.30
T (min/max)	0.55/1.00	0.62/1.00	0.49/0.75
radiation	Mo Kα (graphite monochromated, λ = 0.71073 Å)		
θ range, (deg)	1.89 < θ < 29.41	1.97 < θ < 29.35	2.02 < θ < 29.72
no. of data collected	17940	22824	26959
no. of indep data	1801	1678	1712
no. of obsd rflns (n_o) [$\|F_o\|^2 > 2.0\sigma(\|F\|^2)$]	1165	1485	1482
no. of params refined (n_v)	56	56	56
ext coeff	0.00265(9)	0.00026(6)	0.0007(1)
R_{int}[a]	0.0213	0.0277	0.0763
R (obsd rflns)[b]	0.0183	0.0207	0.0384
R^2_w (obsd rflns)[c]	0.0409	0.0431	0.0955
GOF[d]	1.048	1.095	1.308

[a] $R_{int} = \sum|F_o^2 - \langle F_o^2\rangle|/\sum F_o^2$. [b] $R = \sum(|F_o| - (1/k)F_c|)/\sum|F_o|$. [c] $R^2_w = \{\sum[w(F_o^2 - (1/k)F_c^2)^2]/\sum w|F_o^2|^2]\}^{1/2}$. [d] GOF = $[\sum_w(F_o^2 - (1/k)F_c^2)^2/(n_o - n_v)]^{1/2}$.

4.10.1. Structural Study of Pt_3I_3. The cell constants were refined by least-squares, at the end of the data collection, using reflections up to $2\theta_{max} \leq 58.2°$. The data were collected by using ω scans, in steps of 0.3°. For each of the 1860 collected frames, counting time was 30 s. The least-squares refinement was carried out using anisotropic displacement parameters for all non-hydrogen atoms. The contribution of the hydrogen atom, in their calculated positions, (C−H = 0.96 (Å), B(H) = 1.5B(C_{bonded}) (Å^2)), was included in the refinement using a riding model.

4.10.2. Structural Study of Pt_3Br_3. The cell constants were refined by least-squares, at the end of the data collection, using reflections up to $2\theta_{max} \leq 57.7°$). The data were collected by using ω scans, in steps of 0.3°. For each of the 1500 collected frames, counting time was 30 s. The least-squares refinement was carried out using anisotropic displacement parameters for all non-hydrogen atoms, while the H atoms were included in the refinement as described above.

4.10.3. Structural Study of Pt_3Cl_3. The values of the cell parameters were refined at the end of the data collection using reflections up to $2\theta_{max} \leq 58.7°$. The data were collected by using ω scans, in steps of 0.5°. For each of the 1500 collected frames, counting time was 20 s. The least-squares refinement was carried out using anisotropic displacement parameters for all non-hydrogen atoms while the H atoms were included in the refinement as described above.

4.11. Computational Details. All the calculations were carried out within the Gaussian 09 package.[46] The models used fully matched the experimental compounds, as the substituents at the phosphorus atoms were real Bu^t groups. Initial work by using much simpler PH_2 bridges was dismissed to avoid any underestimation of the steric hindrance effects. In the calculations, the B3LYP functional[29] with standard double-ζ quality LanL2DZ basis set was used for all the elements.[30] Polarization d functions were added on the P and I atoms. For the heavier atoms (Pt and I), the Los Alamos effective core potential was used. All calculations were carried out with the conductor-like polarizable continuum model (CPCM) for a dichloromethane solution.[31] The energy convergence criterion was set at 10^{-7} h. The latter value and the nonoptimal basis set were chosen as a good compromise between the quality of the results and the highly requiring complexity of the full models. Frequency calculations confirmed the nature of any minimum structure. Based on the latter, also the free energy contributions were evaluated for all the structures and were exploited to construct potential energy surfaces, from which the most probable reaction pathways were described. Accompanying qualitative MO arguments have been developed with the CACAO package and its graphic interface.[47]

■ ASSOCIATED CONTENT

Supporting Information

Experimental and calculated redox potentials for the 42e$^-$/43e$^-$ and the 43e$^-$/44e$^-$ redox couples in the series $[Pt_3(CO)_{3-n}I_n]^{(3-n)+/(2-n)+/(1-n)+}$; complete listing of bond lengths and angles for the structures of Pt_3X_3; tables of calculated CO stretchings and of coordinates and the associated thermal parameters of all the optimized structures. This material is available free of charge via the Internet at http://pubs.acs.org.

■ AUTHOR INFORMATION

Corresponding Author

*E-mail: leoni@dcci.unipi.it (P.L.), mealli@iccom.cnr.it (C.M.).

Notes

The authors declare no competing financial interest.

■ ACKNOWLEDGMENTS

This work was supported by the Ministero dell'Istruzione, Universitá e Ricerca (MIUR), Project PRIN2008 No. 2008RFEB3X, and by the Fondazione Cassa di Risparmio di Pisa under the "POLOPTEL" project n. 167/09. The computational work was carried out thanks to the ISCRA-CINECA HP Grants HP10BNL89W, HP10BJ8IKG and HP10BEG2NO. Part of this work was carried out by C.M. and G.M. during a scientific visit at the Research Center For Material Science (RSCM) of the University of Nagoya.

REFERENCES

(1) Chatt, J.; Chini, P. *J. Chem. Soc. A* **1970**, 1538−1541.

(2) (a) Allen, F. H. *Acta Crystallogr.* **2002**, *B58*, 380−388. (b) Bruno, I. J.; Cole, J. C.; Edgington, P. R.; Kessler, M.; Macrae, C. F.; McCabe, P.; Pearson, J.; Taylor, R. *Acta Crystallogr.* **2002**, *B58*, 389−397.

(3) (a) Mingos, D. M. P.; Lin, Z. *J. Chem. Soc., Dalton Trans.* **1988**, 1657−1664. (b) Evans, D. G. *J. Organomet. Chem.* **1988**, *352*, 397−413.

(4) (a) Mingos, D. M. P. *Chem. Soc. Rev.* **1986**, 31−61. (b) Lloyd, B. R.; Bradford, A.; Puddephatt, R. J. *Organometallics* **1987**, *6*, 424−427. (c) Muetterties, E. L.; Rhodin, T. N.; Band, E.; Brucker, C. F.; Pretzer, W. R. *Chem. Rev.* **1979**, *2*, 91−137.

(5) (a) Falvello, L. R.; Fornies, J.; Fortuno, C.; Duran, F.; Martin, A. *Organometallics* **2002**, *21*, 2226−2234. (b) Chaplin, A. B.; Beni, Z.; Hartinger, C. G.; Hamidane, H. B.; Phillips, A. D.; Scopelliti, R.; Dyson, P. J. *J. Cluster Sci.* **2008**, *19*, 295−309. (c) Braunstein, P.; Freyburger, S.; Bars, O. *J. Organomet. Chem.* **1988**, *352*, C29−C33. (d) Stockhammer, A.; Dahmen, K.-H.; Gerfin, T.; Venanzi, L. M.; Gramlich, V.; Petter, W. *Helv. Chim. Acta* **1991**, *74*, 989−992. (e) Sterenberg, B. T.; Jennings, M. C.; Puddephatt, R. J. *Organometallics* **1999**, *18*, 3737−3743. (f) Hao, L.; Xiao, J.; Vittal, J. J.; Puddephatt, R. J. *Organometallics* **1997**, *16*, 2165−2174. (g) Sterenberg, B. T.; Spivak, G. J.; Yap, G. P. A.; Puddephatt, R. J. *Organometallics* **1998**, *17*, 2433−2439. (h) Stadnichenko, R.; Sterenberg, B. T.; Bradford, A. M.; Jennings, M. C.; Puddephatt, R. J. *J. Chem. Soc., Dalton Trans.* **2002**, 1212−1216.

(6) (a) Sterenberg, B. T.; Ramachandran, R.; Puddephatt, R. J. *J. Cluster Sci.* **2001**, *12*, 49−59. (b) Xiao, J.; Hao, L.; Puddephatt, R. J.; Manojlovic-Muir, L.; Muir, K. W. *J. Am. Chem. Soc.* **1995**, *117*, 6316−6326. (c) de Silva, N.; Fry, C. G.; Dahl, L. F. *Dalton Trans.* **2006**, 1051−1059.

(7) (a) Payne, N. C.; Ramachandran, R.; Schoettel, G.; Vittal, J. J.; Puddephat, R. J. *Inorg. Chem.* **1991**, *30*, 4048−4053. (b) King, W. D.; Lukehart, C. M. *J. Cluster Sci.* **1998**, *9*, 107−121. (c) Hao, L.; Xiao, J.; Vittal, J. J.; Puddephatt, R. J.; Manojlovic-Muir, L.; Muir, K. W.; Torabi, A. A. *Inorg. Chem.* **1996**, *35*, 658−666. (d) Jennings, M. C.; Schoettel, G.; Roy, S.; Puddephatt, R. J.; Douglas, G.; Manojlovic-Muir, L.; Muir, K. W. *Organometallics* **1991**, *10*, 580−586. (e) Adams, R. D.; Captain, B.; Beddie, C.; Hall, M. B. *J. Am. Chem. Soc.* **2007**, *129*, 986−1000.

(8) (a) Yamamoto, Y.; Yamazaki, H. *Inorg. Chim. Acta* **1994**, *217*, 121−127. (b) Albinati, A.; Dahmen, K.-H.; Togni, A.; Venanzi, L. M. *Angew. Chem., Int. Ed.* **1985**, *24*, 766−767. (c) Hallam, M. F.; Mingos, D. M. P.; Adatia, T.; McPartlin, M. *J. Chem. Soc., Dalton Trans.* **1988**, 335−340. (d) Mednikov, E. G.; Dahl, L. F. *Dalton Trans.* **2003**, 3117−3125. (e) Tanase, T.; Goto, E.; Takenaka, H.; Horiuchi, T.; Yamamoto, Y.; Kuwabara, J.; Osakada, K. *Organometallics* **2005**, *24*, 234−244.

(9) (a) Calabrese, J. C.; Dahl, L. F.; Chini, P.; Longoni, G.; Martinengo, S. *J. Am. Chem. Soc.* **1974**, *96*, 2614−2626. (b) Hao, L.; Manojlovic-Muir, L.; Muir, K. W.; Puddephatt, R. J.; Spivak, G. J.; Vittal, J. J.; Yufit, D. *Inorg. Chim. Acta* **1997**, *265*, 65−74. (c) Spivak, G. J.; Hao, L.; Vittal, J. J.; Puddephatt, R. J. *J. Am. Chem. Soc.* **1996**, *118*, 225−226. (d) Zacchini, S. *Eur. J. Inorg. Chem.* **2011**, 4125−4145. (e) Femoni, C.; Iapalucci, M. C.; Kaswalder, F.; Longoni, G.; Zacchini, S. *Coord. Chem. Rev.* **2006**, *250*, 1580−1604.

(10) Hao, L.; Spivak, G. J.; Xiao, J.; Vittal, J. J.; Puddephatt, R. J. *J. Am. Chem. Soc.* **1995**, *117*, 7011−7012.

(11) (a) Albinati, A.; Leoni, P.; Marchetti, L.; Rizzato, S. *Angew. Chem., Int. Ed.* **2003**, *42*, 5990−5993. (b) Leoni, P.; Marchetti, F.; Marchetti, L.; Pasquali, M. *Chem. Commun.* **2003**, 2372−2373. (c) Leoni, P.; Marchetti, L.; Mohapatra, S. K.; Ruggeri, G.; Ricci, L. *Organometallics* **2006**, *25*, 4226−4230. (d) Bonaccorsi, C.; Fabrizi de Biani, F.; Leoni, P.; Marchetti, F.; Marchetti, L.; Zanello, P. *Chem.—Eur. J.* **2008**, *14*, 847−856. (e) Albinati, A.; Fabrizi de Biani, F.; Leoni, P.; Marchetti, L.; Pasquali, M.; Rizzato, S.; Zanello, P. *Angew. Chem., Int. Ed.* **2005**, *44*, 5701−5705. (f) Leoni, P.; Marchetti, F.; Marchetti, L.; Pasquali, M.; Quaglierini, S. *Angew. Chem., Int. Ed.* **2001**, *40*, 3617−3618. (g) Fabrizi de Biani, F.; Ienco, A.; Laschi, F.; Leoni, P.; Marchetti, F.; Marchetti, L.; Mealli, C.; Zanello, P. *J. Am. Chem. Soc.* **2005**, *127*, 3076−3089. (h) Leoni, P.; Marchetti, L.; Bonuccelli, V.; Mohapatra, S. K.; Albinati, A.; Rizzato, S. *Chem.—Eur. J.* **2010**, *16*, 9468−9477.

(12) (a) Itazaki, M.; Kitami, O.; Tanabe, M.; Nishihara, Y.; Osakada, K. *J. Organomet. Chem.* **2005**, *690*, 3957−3962. (b) Imhof, D.; Burckhardt, U.; Dahmen, K.-H.; Joho, F.; Nesper, R. *Inorg. Chem.* **1997**, *36*, 1813−1820. (c) Albinati, A.; Balzano, F.; Fabrizi de Biani, F.; Leoni, P.; Manca, G.; Marchetti, L.; Rizzato, S.; Uccello Barretta, G.; Zanello, P. *Inorg. Chem.* **2010**, *49*, 3714−3720. (d) Femoni, C.; Kaswalder, F.; Iapalucci, M. C.; Longoni, G.; Zacchini, S. *Chem. Commun.* **2006**, 2135−2137.

(13) μ-R_2E: (a) Braddock-Wilking, J.; Corey, J. Y.; French, L. M.; Choi, E.; Speedie, V. J.; Rutherford, M. F.; Yao, S.; Xu, H.; Rath, N. P. *Organometallics* **2006**, *25*, 3974−3988. (b) Jeffery, J. C.; Moore, I.; Murray, M.; Stone, F. G. A. *J. Chem. Soc., Dalton Trans.* **1982**, 1741−1747. (c) Campbell, G. K.; Hitchcock, P. B.; Lappert, M. F.; Misra, M. C. *J. Organomet. Chem.* **1985**, *289*, C1−C4. (d) Osakada, K.; Tanabe, M.; Tanase, T. *Angew. Chem., Int. Ed.* **2000**, *39*, 4053−4055. μ-RNC: (e) Briant, C. E.; Gilmour, D. I.; Mingos, D. M. P.; Wardle, R. W. M. *J. Chem. Soc., Dalton Trans.* **1985**, 1693−1698. (f) Haggitt, J. L.; Mingos, D. M. P. *J. Organomet. Chem.* **1993**, *462*, 365−374. μ-CO: (g) Burrow, R. A.; Farrar, D. H.; Irwin, J. J. *Inorg. Chim. Acta* **1991**, *181*, 65−72. (h) Poverenov, E.; Gandelman, M.; Shimon, L. J. W.; Rozenberg, H.; Ben-David, Y.; Milstein, D. *Organometallics* **2005**, *24*, 1082−1090. μ-SO_2: (i) Bott, S. G.; Hallam, M. F.; Ezomo, O. J.; Mingos, D. M. P.; Williams, I. D. *J. Chem. Soc., Dalton Trans.* **1988**, 1461−1466. (j) Heyke, O.; Maichle, C.; Hubener, R.; Lorenz, I.-P. *Z. Anorg. Allg. Chem.* **1993**, *619*, 1793−1800.

(14) Ferguson, G.; Lloyd, B. R.; Puddephatt, R. J. *Organometallics* **1986**, *5*, 344−348.

(15) (a) Hallam, M. F.; Howells, N. D.; Mingos, D. M. P.; Wardle, R. W. M. *J. Chem. Soc., Dalton Trans.* **1985**, 845−850. (b) Mingos, D. M. P.; Williams, I. D.; Watson, M. J. *J. Chem. Soc., Dalton Trans.* **1988**, 1509−1516. (c) Albinati, A.; Carturan, G.; Musco, A. *Inorg. Chim. Acta* **1976**, *16*, L3−L4.

(16) (a) Bradford, A. M.; Kristof, E.; Rashidi, M.; Yang, D.-S.; Payne, N. C.; Puddephatt, R. J. *Inorg. Chem.* **1994**, *33*, 2355−2363. (b) Ramachandran, R.; Yang, D.-S.; Payne, N. C.; Puddephatt, R. J. *Inorg. Chem.* **1992**, *31*, 4236−4240. (c) Jennings, M. C.; Puddephatt, R. J.; Manojlovic-Muir, L.; Muir, K. W.; Mwariri, B. N. *Organometallics* **1992**, *11*, 4164−4166. (d) Bradford, A. M.; Douglas, G.; Manojlovic-Muir, L.; Muir, K. W.; Puddephatt, R. J. *Organometallics* **1990**, *9*, 409−416. (e) Puddephatt, R. J.; Rashidi, M.; Vittal, J. J. *J. Chem. Soc., Dalton Trans.* **1991**, 2835−2843. (f) Holah, D. G.; Hughes, A. N.; Krysa, E.; Spivak, G. J.; Havighurst, M. D.; Magnuson, V. R. *Polyhedron* **1997**, *16*, 2353−2359.

(17) Leoni, P.; Marchetti, F.; Pasquali, M.; Marchetti, L.; Albinati, A. *Organometallics* **2002**, *21*, 2176−2182.

(18) Itazaki, M.; Nishihara, Y.; Osakada, K. *Organometallics* **2004**, *23*, 1610−1621.

(19) (a) Cavazza, C.; Fabrizi de Biani, F.; Funaioli, T.; Leoni, P.; Marchetti, F.; Marchetti, L.; Zanello, P. *Inorg. Chem.* **2009**, *48*, 1385−1397. (b) Leoni, P.; Manetti, S.; Pasquali, M.; Albinati, A. *Inorg. Chem.* **1996**, *35*, 6045−6052. (c) Fabrizi de Biani, F.; Manca, G.; Marchetti, L.; Leoni, P.; Bruzzone, S.; Guidotti, C.; Atrei, A.; Albinati, A.; Rizzato, S. *Inorg. Chem.* **2009**, *48*, 10126−10137.

(20) (a) Bender, R.; Braunstein, P.; Bouaoud, S.-E.; Merabet, N.; Rouag, D.; Zanello, P.; Fontani, M. *New J. Chem.* **1999**, *23*, 1045−1047. (b) Taylor, N. J.; Chieh, P. C.; Carty, A. J. *Chem. Commun.* **1975**, 448−449. (c) Bender, R.; Braunstein, P.; Dedieu, A.; Ellis, P. D.; Huggins, B.; Harvey, P. D.; Sappa, E.; Tiripicchio, A. *Inorg. Chem.* **1996**, *35*, 1223−1234.

(21) (a) Hao, L.; Jobe, I. R.; Vittal, J. J.; Puddephatt, R. J. *Organometallics* **1995**, *14*, 2781−2789. (b) Bradford, A. M.; Puddephatt, R. J.; Douglas, G.; Manojlovic-Muir, L.; Muir, K. W. *Organometallics* **1990**, *9*, 1579−1585. (c) Jennings, M. C.; Manojlovic-Muir, L.; Puddephatt, R. J. *J. Am. Chem. Soc.* **1989**, *111*, 745−746. (d) Douglas, G.; Manojlovic-Muir, L.; Muir, K. W.; Rashidi, M.;

Anderson, C. M.; Puddephatt, R. J. *J. Am. Chem. Soc.* **1987**, *109*, 6527−6528. (e) Ling, S. S. M.; Hadj-Bagheri, N.; Manojlovic-Muir, L.; Muir, K. W.; Puddephatt, R. J. *Inorg. Chem.* **1987**, *26*, 231−235.

(22) (a) Longato, B.; Bandoli, G.; Dolmella, A. *Eur. J. Inorg. Chem.* **2004**, 1092−1099. (b) Novio, F.; Mas-Balleste, R.; Gallardo, I.; Gonzalez-Duarte, P.; Lledos, A.; Vila, N. *Dalton Trans.* **2005**, 2742−2753. (c) Tzeng, B.-C.; Chan, S.-C.; Chan, M. C. W.; Che, C.-M.; Cheung, K. K.; Peng, S.-M. *Inorg. Chem.* **2001**, *40*, 6699−6704. (d) Albrecht, C.; Schwieger, S.; Bruhn, C.; Wagner, C.; Kluge, R.; Schmidt, H.; Steinborn, D. *J. Am. Chem. Soc.* **2007**, *129*, 4551−4566. (e) Ruiz, J.; Rodriguez, V.; Perez, A.; Lopez, G.; Bautista, D. *J. Organomet. Chem.* **2004**, *689*, 2080−2086. (f) Jeram, S.; Henderson, W.; Nicholson, B. K.; Hor, T. S. A. *J. Organomet. Chem.* **2006**, *691*, 2827−2838. (g) Ara, I.; Falvello, L. R.; Fernandez, S.; Fornies, J.; Lalinde, E.; Martin, A.; Moreno, M. T. *Organometallics* **1997**, *16*, 5923−5937. (h) Sellmann, D.; Haussinger, D.; Heinemann, F. W. *Eur. J. Inorg. Chem.* **1999**, 1715−1725.

(23) (a) Yamaguchi, T.; Nishimura, N.; K-i. Shirakura, K-i.; Ito, T. *Bull. Chem. Soc. Jpn.* **2000**, *73*, 775−784. (b) Yamaguchi, T.; Nishimura, N.; Ito, T. *J. Am. Chem. Soc.* **1993**, *115*, 1612−1613.

(24) El-Hallag, I. S. *J. Chil. Chem. Soc.* **2010**, *55*, 67−73.

(25) Cramer, C. J.; Truhlar, D. G. *Chem. Rev.* **1999**, *99*, 2161−2200.

(26) Mealli, C. *J. Am. Chem. Soc.* **1985**, *107*, 2245−2253.

(27) (a) Beni, Z.; Ros, R.; Tassan, A.; Scopelliti, R.; Roulet, R. *Dalton Trans.* **2005**, 315−325. (b) Archambault, C.; Bender, R.; Bouaoud, S.-E.; Braunstein, P.; Rouag, D.; Golhen, S.; Ouahab, L. *Chem. Commun.* **2001**, 849−850. (c) Schuh, W.; Wachtler, H.; Laschober, G.; Kopacka, H.; Wurst, K.; Peringer, P. *Chem. Commun.* **2000**, 1181−1182.

(28) Occasionally, both organic and inorganic compounds may exhibit the so-called redox potential inversion so that the second electron addition/removal is easier than the first one. This is commonly ascribed to dramatic structural changes induced by a first redox reaction, which can facilitate the subsequent redox reaction. See, as recent examples, the following references and references therein: Sakamoto, R.; Tsukada, S.; Nishihara, H. *Dalton Trans.* **2012**, *41*, 10123−10135. Muratsugu, S.; Sodeyama, K.; Kitamura, F.; Tsukada, S.; Tada, M.; Tsuneyuki, S.; Nishihara, H. *Chem. Sci.* **2011**, *2*, 1960−1968.

(29) Becke, A. D. *J. Chem. Phys.* **1993**, *98*, 5648−5652.

(30) (a) Dunning, T. H., Jr..; Hay, P. J. In *Modern Theoretical Chemistry*; Schaefer, H. F., III, Ed.; Plenum: New York, 1976; Vol. 3, pp 1−28. (b) Hay, P. J.; Wadt, W. R. *J. Chem. Phys.* **1985**, *82*, 270−283. (c) Wadt, W. R.; Hay, P. J. *J. Chem. Phys.* **1985**, *82*, 284−298.

(31) (a) Barone, V.; Cossi, M. *J. Phys. Chem. A* **1998**, *102*, 1995−2001. (b) Cossi, M.; Rega, N.; Scalmani, G.; Barone, V. *J. Comput. Chem.* **2003**, *24*, 669−681.

(32) (a) Hirva, P.; Haukka, M.; Jakonen, M.; Moreno, M. A. *J. Mol. Model.* **2008**, *14*, 171−181. (b) Lombardi, J. R.; Davis, B. *Chem. Rev.* **2002**, *102*, 2431−2460. (c) Barden, C. J.; Rienstra-Kiracofe, J. C.; Schaefer, H. F., III *J. Chem. Phys.* **2000**, *113*, 690−700. (d) Yanagisawa, S.; Tsuneda, T.; Hirao, K. *J. Chem. Phys.* **2000**, *112*, 545−553.

(33) Bender, R.; Braunstein, P.; Tiripicchio, A.; Tiripicchio-Camellini, M. *Angew. Chem., Int. Ed. Engl.* **1985**, *24*, 861−862.

(34) The correlation for mixed CO/I^- redox derivatives is less straightforward in view of the lower symmetry ($D_{3h} \rightarrow C_{2v}$), which induces significant orbital mixing with effects on Pt−P linkages.

(35) (a) Stock, J. T., Orna, M. V., Eds. *Electrochemistry, past and present*; American Chemical Society: Washington, DC, 1989. (b) Wahl, D. *Galvanotechnik* **2005**, *96*, 1820−1828.

(36) One reviewer pointed out that the released CO molecule would participate in high yield substitution processes, instead of being lost from the solution. Possibly, CO remains engaged in intermolecular interactions, which may allow its exchange between different Pt_3 units. Although the complex mechanism was not explored, it may not be excluded that the $\{\mathbf{Pt_3(CO)_2I_2}\}$ adduct transfers one CO ligand to its precursor $\{\mathbf{Pt_3(CO)_2I}\}^+$ giving $\{\mathbf{Pt_3(CO)_3I}\}^+$ and $\{\mathbf{Pt_3(CO)I_2}\}$.

(37) (a) Hoffmann, R.; Lipscomb, W. N. *J. Chem. Phys.* **1962**, *37*, 2872−2883. (b) Hoffmann, R.; Lipscomb, W. N. *J. Chem. Phys.* **1962**, *37*, 3489−3493.

(38) Isse, A. A.; Gennaro, A. *J. Phys. Chem. B* **2010**, *114*, 7894−7899.

(39) (a) The coupling constants [$^1J_{PtPt}$, $^2J_{PP}$, $^1J_{PtP}$ and $^2J_{PtP}$] can be accurately determined through simulation[39b] which reproduces nicely the complex pattern of the higher order satellites of the signals of P and Pt. (b) Budzelaar, P. H. M. *gNMR, version 5.0.6.0*; Adept Scientific plc: Herts, U.K., 2006.

(40) *BrukerAXS, SAINT*; Integration Software; Bruker Analytical X-ray Systems: Madison, WI, 1995.

(41) Sheldrick, G. M. *SADABS*, Program for Absorption Correction; University of Göttingen: Göttingen, Germany, 1996.

(42) Sheldrick, G. M. *Acta Crystallogr.* **2008**, *A64*, 112−122.

(43) *International Tables for X-ray Crystallography*; Wilson, A. J. C., Ed.; Kluwer Academic Publisher: Dordrecht, The Netherlands, 1992; Vol. *C*.

(44) (a) Farrugia, L . J. *J. Appl. Crystallogr.* **1997**, *30*, 565. (b) Farrugia, L . J. *J. Appl. Crystallogr.* **1999**, *32*, 837−838.

(45) *Mercury CSD 3.0.1 (Build RC6)*; The Cambridge Crystallographic Data Center: Cambridge, U.K., 2012.

(46) Frisch, M. J.; Trucks, G. W.; Schlegel, H. B.; Scuseria, G. E.; Robb, M. A.; Cheeseman, J. R.; Scalmani, G.; Barone, V.; Mennucci, B.; Petersson, G. A.; Nakatsuji, H.; Caricato, M.; Li, X.; Hratchian, H. P.; Izmaylov, A. F.; Bloino, J.; Zheng, G.; Sonnenberg, J. L.; Hada, M.; Ehara, M.; Toyota, K.; Fukuda, R.; Hasegawa, J.; Ishida, M.; Nakajima, T.; Honda, Y.; Kitao, O.; Nakai, H.; Vreven, T.; Montgomery, J. A., Jr.; Peralta, J. E.; Ogliaro, F.; Bearpark, M.; Heyd, J. J.; Brothers, E.; Kudin, K. N.; Staroverov, V. N.; Kobayashi, R.; Normand, J.; Raghavachari, K.; Rendell, A.; Burant, J. C.; Iyengar, S. S.; Tomasi, J.; Cossi, M.; Rega, N.; Millam, J. M.; Klene, M.; Knox, J. E.; Cross, J. B.; Bakken, V.; Adamo, C.; Jaramillo, J.; Gomperts, R.; Stratmann, R. E.; Yazyev, O.; Austin, A. J.; Cammi, R.; Pomelli, C.; Ochterski, J. W.; Martin, R. L.; Morokuma, K.; Zakrzewski, V. G.; Voth, G. A.; Salvador, P.; Dannenberg, J. J.; Dapprich, S.; Daniels, A. D.; Farkas, Ö.; Foresman, J. B.; Ortiz, J. V.; Cioslowski, J.; Fox, D. J. *Gaussian 09, Revision A.1*; Gaussian, Inc.: Wallingford, CT, 2009.

(47) (a) Mealli, C.; Proserpio, D. M. *J. Chem. Educ.* **1990**, *67*, 399−403. (b) Mealli, C.; Ienco, A.; Proserpio, D. M. *Book of Abstracts of the XXXIII ICCC*; CNR, Area della Ricerca di Firenze: Florence; 1998, p 510.